



Confinement effects on compressive and ballistic performance of ceramics: a review

Rui Zhang , Bin Han & Tian Jian Lu

To cite this article: Rui Zhang , Bin Han & Tian Jian Lu (2020): Confinement effects on compressive and ballistic performance of ceramics: a review, International Materials Reviews, DOI: [10.1080/09506608.2020.1830665](https://doi.org/10.1080/09506608.2020.1830665)

To link to this article: <https://doi.org/10.1080/09506608.2020.1830665>



Published online: 13 Oct 2020.



Submit your article to this journal [↗](#)



Article views: 67



View related articles [↗](#)



View Crossmark data [↗](#)



Confinement effects on compressive and ballistic performance of ceramics: a review

Rui Zhang^{a,b,c}, Bin Han^b and Tian Jian Lu^{c,d}

^aState Key Laboratory for Strength and Vibration of Mechanical Structures, Xi'an Jiaotong University, Xi'an, People's Republic of China;

^bSchool of Mechanical Engineering, Xi'an Jiaotong University, Xi'an, People's Republic of China; ^cNanjing Center for Multifunctional Lightweight Materials and Structures (MLMS), Nanjing University of Aeronautics and Astronautics, Nanjing, People's Republic of China;

^dState Key Laboratory of Mechanics and Control of Mechanical Structures, Nanjing University of Aeronautics and Astronautics, Nanjing, People's Republic of China

ABSTRACT

Ceramic materials have been extensively used as armour materials for nearly 50 years and continue to attract great interest in the field of defense technology. As confinement is crucial for ceramics to achieve enhanced performance, it has become indispensable in ceramic armour systems. This review aims to explore the effects of a wide variety of confinement on ceramic performance, so as to provide scientific insights for further exploration and development of ceramic materials and ceramic-based armour systems for both researchers and engineers. This work first characterises multiaxial compressive experiments of ceramics, explores confinement-induced brittle to ductile transition, and presents pressure-dependent micromechanical and phenomenological constitutive models. Subsequently, the change of fracture mode under compression and the reduction of damage extent under projectile impact are separately discussed. Enhancement in ballistic performance by confining and prestressing ceramics is also introduced, with corresponding physical mechanisms explored. Last but not least, insights into future opportunities and challenges are presented.

ARTICLE HISTORY

Received 17 February 2020
Accepted 25 September 2020

KEYWORDS

Ceramic; confinement;
prestressing; compression;
penetration

Introduction

Advanced ceramics with unique combinations of mechanical, electrical and thermal properties have exhibited great superiority in electronic devices [1–3], bone substitutes [4], structural components [5], cutting tools [6] and thermal protections [7]. Moreover, the concept of ceramic composite armour was proposed in 1960s, which grew fast with increasing demands of light weight and high ballistic performance [8,9]. Presently, ceramics are one of the most important materials in high-performance armour systems, offering the best potential for future protection requirements [10].

Typically, the ceramics exploited in the construction of penetration resistant systems have the characteristics of low density, high strength and high hardness, e.g. alumina (Al_2O_3), silicon carbide (SiC), and boron carbide (B_4C). By combining ceramics with metals or fibre-reinforced composites, lightweight ceramic composite armours with extraordinary ballistic performance have been developed in the last decades. To this end, extensive experimental [11–14], numerical [15–17] and theoretical studies [18–22] have been carried out. Simultaneously, the

focus has also been placed upon the mechanical properties of ceramics to provide an insightful understanding of their response mechanisms during penetration [23,24], the influence of microstructural properties [25–27], the development of damage under compressive stressing [28,29], and the relationship between material properties and ballistic performance [30–32].

Just ahead of an impacting projectile, the ceramic is in the state of multiaxial compression [33]. Unlike ductile metals, uniaxial compressive behaviour cannot fully represent the compressive properties of a ceramic, for its strength is dominated by hydrostatic pressure. Therefore, characterising the response of the ceramic under multiaxial compression is not only the basis for developing its constitutive relationship, but also deepens the understanding of its ballistic performance. In order to achieve multiaxial loading, pressures in other directions rather than the main compressive direction are usually induced by confinements, which are commonly referred to as the confining pressure.

The ballistic resistance of an armour ceramic is dependent not only upon its material properties, but also upon confinement built into the armour system

CONTACT Bin Han hanbinghost@xjtu.edu.cn School of Mechanical Engineering, Xi'an Jiaotong University, Xinan 710049, People's Republic of China; Tian Jian Lu tjlu@nuaa.edu.cn State Key Laboratory of Mechanics and Control of Mechanical Structures, Nanjing University of Aeronautics and Astronautics, Nanjing 210016, People's Republic of China; Nanjing Center for Multifunctional Lightweight Materials and Structures (MLMS), Nanjing University of Aeronautics and Astronautics, Nanjing 210016, People's Republic of China

[10]. Confinement in ballistic experiments may be broadly classified into two categories: ‘impedance confinement’ and ‘pressure confinement’ [34]. Impedance confinement refers to the use of materials with different wave impedances to restrict ceramic deformation, the ceramic being pressure-free before penetration. Pressure confinement refers to the application of compression-induced prestress on the ceramic before penetration.

In the current review, the effects of varying confinements on the compressive and ballistic performance of ceramics, along with the underlying mechanisms are systematically explored. First, common brittle failures of ceramics caused by defects and the transition of brittle to ductile failure are discussed, with relevant experimental techniques and constitutive models summarised. Subsequently, fracture modes of ceramics under different stress states are compared, and reduced damage in confined ceramics under projectile impact is presented. Lastly, the enhanced ballistic performance of ceramics achieved via confining and prestressing is elucidated. Insights into challenges and future perspectives are also provided.

Stress-state controlled compressive behaviour

Defect-controlled brittle failure

As chemical bonds in ceramics are dominated by ionic bonds and covalent bonds, the bonding energy between atoms is typically much higher than metals, resulting in the higher elastic modulus and theoretical strength of ceramics. However, pores, inclusions and other defects are commonly found in ceramics, as shown in [Figure 1](#), which act as the source of cracks due to stress concentration in the presence of external loading. Cracks in ceramics usually grow unstably under tension while stably under compression, and the final failure occurs when the cracks extend to a certain length and begin to interact and merge. Therefore, the failure strength of ceramics in compression is much greater than that in tension, but still far below the theoretical strength. As the failure is controlled by defects, the stress in a ceramic crystal cannot reach a sufficiently high value to induce plastic deformation so that brittle fracture typically occurs in ceramics.

Consider next the relationship between defects and the sintering process. Sintering is usually employed to obtain dense solid from ceramic powders, and different sintering processes result in different microstructures. In general, the sintering process can be classified into four categories: pressureless sintering [35,36], hot pressing (HP) or hot isostatic pressing (HIP) [37–40], reaction sintering [41,42], and spark plasma sintering (SPS) [43–45].

Pressureless sintering is often performed at higher temperatures, with additives sometimes employed to reduce the sintering temperature. Compared to other processes, pressureless sintered ceramics usually have higher porosities and larger grain sizes, and the addition of additives also lead to the presence of second phase at grain boundaries ([Figure 1\(a\)](#)). Notably, reaction sintering is used to fabricate SiC, conducted by reactively infiltrating a preform consisting of SiC and carbon with molten Si. Reaction bonded SiC exhibits no porosity, but its grains are large and the grain boundaries would be occupied by residual silicon that does not participate in the reaction, as shown in [Figure 1\(b\)](#). In hot pressing or hot isostatic pressing, the ceramics are subjected to both elevated temperature and pressure. Under sufficiently high pressure, the porosity can be close to zero and the grain size is small. But such techniques are perceived as expensive, with low production efficiency. Note that the graphite, boron nitride and other impurities in [Figure 1\(c\)](#) are not introduced by the sintering process, which can be primitively detected in the B₄C powders from manufacturers [46]. Significant features of spark plasma sintering (SPS) include high heating rate, high pressure, and current sensitivity. With low energy consumption, short sintering time and the potential to obtain fine-grained dense ceramics ([Figure 1\(d\)](#)), the SPS has become an attractive processing approach.

The size and number of defects in a ceramic affect significantly its strength. Ceramics with higher density, smaller grain size and cleaner grain boundaries generally show higher strength in compression [47]. Upon comparing the characteristics of different sintering process, it can be deduced that ceramics fabricated via the HP, HIP and SPS approaches possess advantages in mechanical performance.

Mechanical responses in multiaxial experiments

The compressive response of a ceramic is related to the stress state. For theoretical modelling, constitutive relations need to be established through multiaxial compression experiments, which are usually carried out by applying confining pressure. Commonly applied confinement techniques are summarised in [Table 1](#). This subsection would describe the experimental phenomena and the effects of confining pressure on ceramic strength. In terms of strain rate employed, the discussion is divided into quasi-static and dynamic experiments.

Quasi-static experiments

Hydraulic pressure vessel ([Table 1\(a\)](#)) has been widely used to apply triaxial quasi-static compression on geologic materials [50,51], and can also be used to carry

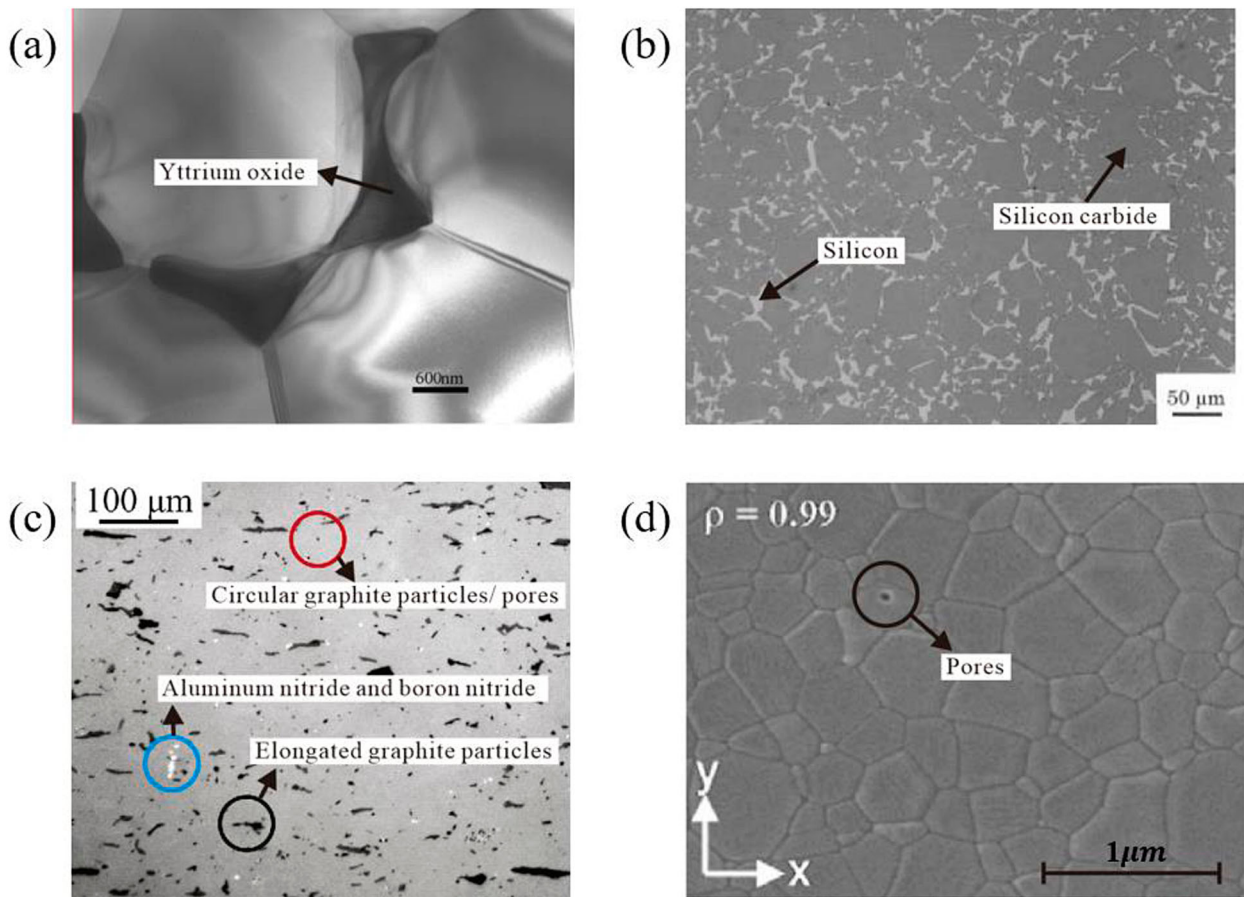


Figure 1. Representative microstructures of (a) pressureless sintered aluminium nitride (AlN) [48], (b) reaction bonded silicon carbide (SiC) [42], (c) hot pressed boron carbide (B_4C) [49], and (d) spark plasma sintered alumina (Al_2O_3) [44].

out triaxial compression tests with ceramics. In the cylindrical vessel, the hydraulic fluid exerts different constant fluid pressures on the specimen, while the axial load is applied by the piston and anvil. To generate moderately large confining pressure, the technique of thick confinement sleeve (Table 1(b)) is developed. The cylindrical specimen is compressed with the constraint by the thick steel sleeve, and the confining pressure can be determined from the strain of steel with a simple elastic calculation [52–54]. With the compressive stress taken as positive, the axial stress in the forgoing two confinement techniques is denoted as σ_1 , and the confining pressure is $\sigma_2 = \sigma_3$ (due to cylindrical symmetry).

Using the hydraulic pressure vessel, Wilkins et al. [9] performed triaxial compression tests on Al_2O_3 , BeO and B_4C , and found that the shear strength $((\sigma_1 - \sigma_3)/2)$ of the three ceramics all increases with confining pressure. In addition, it was found that BeO behaves like ductile metal, sustaining a large strain up to 10% at a confining pressure of 350 MPa or higher, whereas Al_2O_3 and B_4C are brittle even when the confining pressure is as high as 1.6 GPa. Heard and Cline [55] also reported the transition from brittle to ductile for BeO and AlN at different confining pressures, but failed to obtain the transition point of Al_2O_3 . Chocron et al. [56] tested predamaged

B_4C using both the pressure vessel and the thick steel sleeve, and concluded that the failure strength of the predamaged B_4C is pressure-dependent.

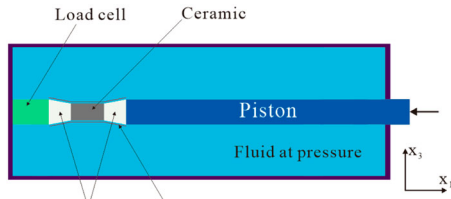
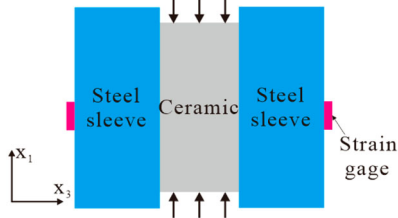
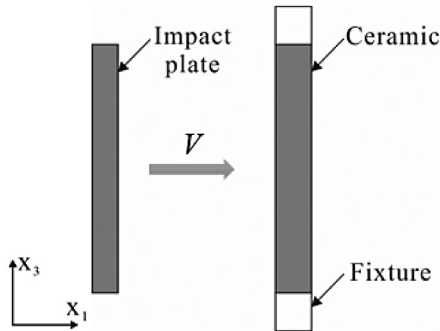
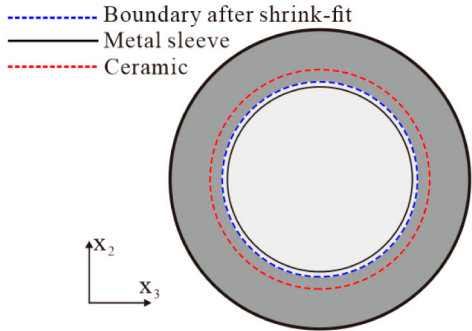
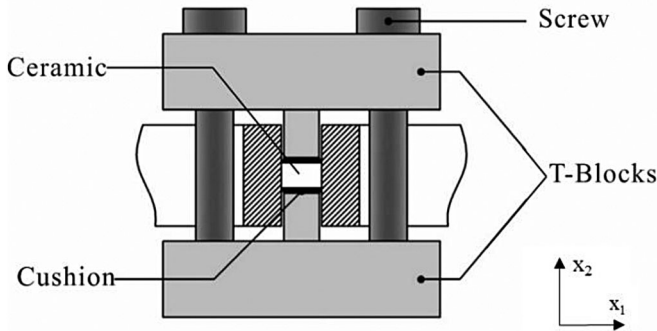
Figure 2 illustrates the influence of confining pressure on the compressive response of a ceramic. Under uniaxial compression, the ceramic exhibits a typical brittle response. In the presence of confining pressure, its compressive strength is increased, with a residual strength retained due to friction (more details presented in Subsection 3.1). If the confining pressure is sufficiently high, the ceramic is likely to behave like ideal elastoplastic materials.

Existing experiments of multiaxial quasi-static compression can be used to characterise the effect of confining pressure on the strength of a range of ceramic materials. For ceramics with higher compressive strength (e.g. Al_2O_3 and B_4C), however, it may be difficult to observe ductile deformation in experiments because the confining pressure achieved with commonly applied confinement techniques is often insufficient.

Dynamic experiments

Studying the dynamic response of ceramics is of great significance for applications in the field of impact protection. Planar impact (Table 1(c)) is an effective method to study the dynamic compressive properties

Table 1. Confinement techniques for multiaxial compression experiments.

Number	Experimental technique	Illustration	Confining pressure (GPa) ^a	Ref.
a	Hydraulic pressure vessel		1.6	[9,50,51,55,56]
b	Thick confinement sleeve		1.0	[52–54,56]
c	Planar impact		8.8	[57–65]
d	Shrink-fit confinement		0.6	[47,67–72]
e	Planar confinement		0.7	[48,73,74]

^aMaximum value measured in the references cited.

of materials at ultra-high strain rates (10^4 – 10^5 s⁻¹), and is usually used to characterise ceramics [57,58]. In planar impact, a projectile plate is used to impact the ceramic target plate and generate a compressive wave of uniaxial strain, with the lateral displacements equal to zero, i.e. $\varepsilon_2 = \varepsilon_3 = 0$. During the impact experiment, histories of particle velocity at the non-impact surface of the ceramic are measured. Dynamic

stresses and strains can be determined through further computational and analytical studies from the obtained profiles. Figure 3(a) displays two typical compressive profiles of alumina oxide with different peak pressures [59]. The initial linear segments of the two profiles correspond to the elastic precursors: the axial stress amplitude of the elastic precursor is denoted as the Hugoniot elastic limit (HEL) and the

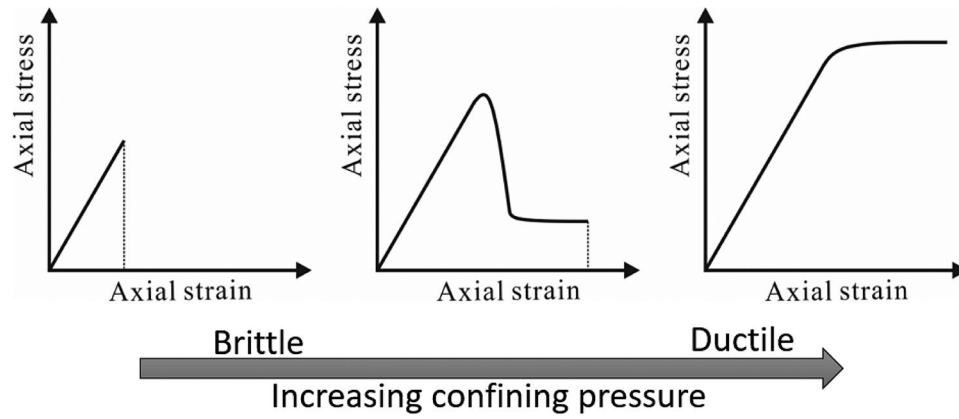


Figure 2. Axial compressive response of ceramics: transition from brittle to ductile with increasing confining pressure.

corresponding velocity amplitude as V_{HEL} . As the axial stress exceeds the HEL, inelastic deformation occurs in the ceramic and the curves are no longer linear. Below the HEL, the confining pressure is dependent upon the axial stress, equalling to $\sigma_3 = \nu\sigma_1/(1 - \nu)$. Typically, high confining pressure can be achieved with planar impact at high strain rates.

Chen et al. [60,61] observed changes in micro deformation around the HEL, as shown in Figure 3 (b). When the shock compressive stress does not exceed the HEL, stress concentrations in the vicinity of grain boundaries may cause the formation of dislocations, which are localised and do not affect the overall elastic response. Above the HEL, when the confining pressure is sufficiently high, a large number of deformation twins are observed and global plastic deformation is activated, leading to an inelastic response. Zaretsky and Kanel [62] also demonstrated that confining stress at the HEL leads to a ductile response of Al_2O_3 . It was further found that the equivalent stress remains constant above the HEL for AlN [63], Al_2O_3 [64] and SiC [65]. Therefore, confining pressure at the HEL may be considered as the key reason for the transition from brittle to ductile under one-dimensional strain shock compression.

While split Hopkinson pressure bar (SHPB) is currently the most popular technique for measuring the stress-strain response of materials at strain rates of $10^2\text{--}10^3\text{ s}^{-1}$ [66], confining pressure can be introduced by modifying the SHPB. Based on the SHPB technique, Chen and Ravichandran [67–69] developed an experimental method to investigate the multi-axial dynamic compression of ceramics, as shown in Table 1(d). Confining pressure was applied by achieving a shrinkage fit between a metal sleeve and the cylindrical ceramic specimen. Impact tests with the assembly were then carried out using the modified split Hopkinson pressure bar. Experimental results for AlN showed that its shear strength increases with increasing strain rate and confining pressure. On a separate front, micro Raman spectroscopy was adopted to quantify the confining pressure in zirconium diboride-silicon carbide ($\text{ZrB}_2\text{--SiC}$) under either quasi-static or dynamic compression [70,71]. The results listed in Table 2 indicate that the confining pressure can increase both the quasi-static and dynamic compressive strength of $\text{ZrB}_2\text{--SiC}$ significantly. Lankford et al. [47,72] conducted compressive experiments on Al_2O_3 at various strain rates under a wide range of confining pressure. It was found that

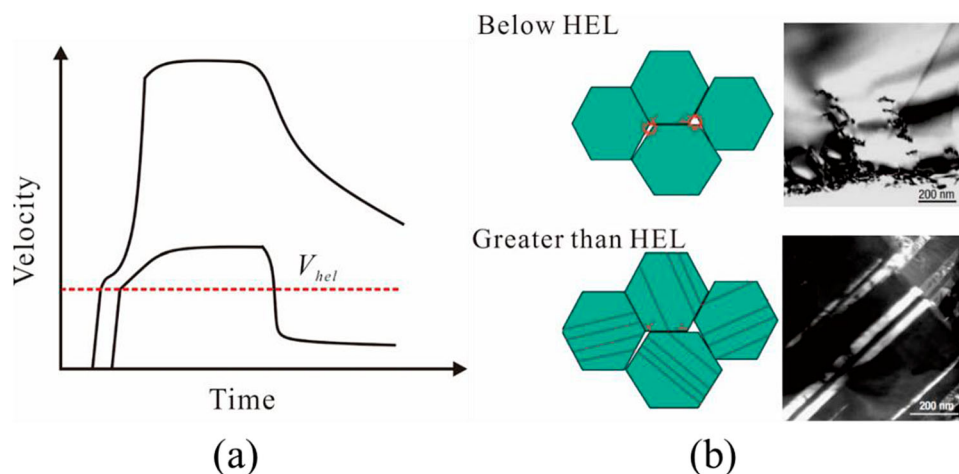


Figure 3. (a) Shock wave profiles for alumina [59] and (b) relationship between micro deformation and HEL (Hugoniot elastic limit) [60].

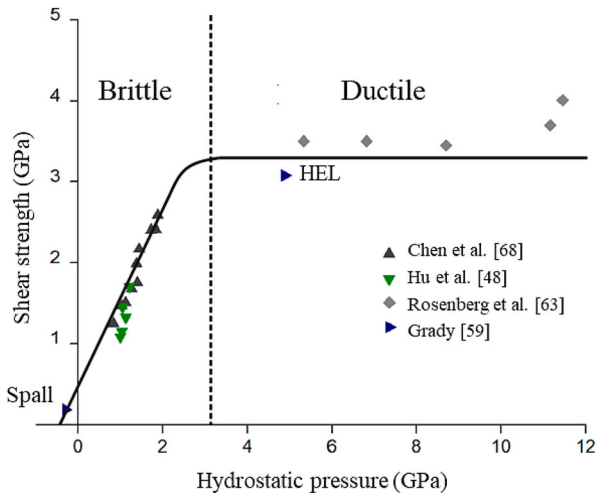
Table 2. Results of confined ZrB₂-SiC under quasi-static and dynamic compression [70].

Quasi-static compression $\dot{\epsilon}_{avg} = 10^{-4} s^{-1}$			Dynamic compression $\dot{\epsilon}_{avg} = 10^2 s^{-1}$		
Confining pressure (GPa)	Peak strength (GPa)	Residual strength (GPa)	Confining pressure (GPa)	Peak strength (GPa)	Residual strength (GPa)
0	0.857	0	0	2.30	0
0.152	3.23	0.8	0.151	5.40	1.6
0.166	3.30	1.5	0.164	6.21	2.2
0.195	3.98	2.2	0.191	7.30	2.9
0.314	5.60	3.3	0.306	9.04	3.9

plastic flow could occur at all strain rates if the confining pressure is sufficiently high to prevent premature failure via micro-fracture.

In addition to triaxial dynamic compression, another technique based on the SHPB was developed to impose planar confinement on a prismatic specimen [73]. Damage evolution of the specimen can be observed during the process of biaxial loading. In this technique, the confining pressure is only exerted along the x_2 -direction, i.e. $\sigma_3 = 0$. Subsequently, the planar confinement was employed to study the response of different ceramics [74]. Under biaxial dynamic compression, the enhancement of ceramic strength is not as significant as that under triaxial dynamic loading. The fracture modes are also different, which will be discussed at length in subsection 3.1.

The techniques used in the modified SHPB can simultaneously control both the confining pressure and the applied dynamic axial stress, although the confining pressure is static and relatively small. Relationship between the dynamic strength of ceramics and the hydrostatic pressure $p = (\sigma_1 + \sigma_2 + \sigma_3)/3$ can be obtained by summarising the results from different experiments, with the strain rates ignored. Figure 4 presents the available data of dynamic experiments for AlN, including the results of planar impact by Grady [59] and Rosenberg et al. [63], the results of modified SHPB experiments by Chen et al. [68] and Hu et al. [48]. It is indicated that the shear strength of

**Figure 4.** Shear strength of AlN plotted as a function of hydrostatic pressure under dynamic loading conditions.

AlN increases linearly with hydrostatic pressure less than 2.5 GPa, gradually approaching a constant when the hydrostatic pressure exceeds 3 GPa. Similar to ductile metals, the strength of ceramics under high hydrostatic pressure (larger than 3 GPa) is pressure-independent, and the transition from brittle to ductile occurs. The results of Figure 4 also show that the shear strength increases again when the hydrostatic pressure exceeds 11 GPa, probably due to phase transition of AlN, a subject not discussed in the current review.

Constitutive models

Micromechanical models

For brittle materials like ceramics, a number of micromechanical models have been proposed to interpret their mechanical responses under compression. Given a set of elastic properties, defect population and stress state, micromechanical models based upon failure mechanisms (e.g. initiation and propagation of cracks) are employed to construct stress-strain constitutive relationships and predict the final failure strength. Built upon the mechanics of tensile microcracks, Costin [75] developed a continuum damage model, but the cracks growth model assumed by Costin does not conform to real physical processes. Inspired by microscopic observations, Ashby and Hallam [76,77] and Horii and Nasser [78] independently developed the wing-crack model, with the initiation, growth and interaction of cracks accounted for. In this model, the wing cracks are assumed to nucleate from the tips of pre-existing inclined microcracks and grow in the direction of maximum compression, as illustrated in Figure 5(a). The criterion for the initiation of wing cracks can be expressed as:

$$\sigma_1 = c_1 \sigma_3 + \sigma_0 \quad (1)$$

where σ_1 is the critical axial stress, σ_3 is the confining stress ($\sigma_3 = \sigma_2$), and c_1 and σ_0 are material properties related to the coefficient of friction and fracture toughness K_{IC} . Once initiated, the wing cracks are expected to grow due to local tensile force F_3 generated by frictional sliding of pre-existing cracks. In addition, crack interaction is considered by introducing the internal stress and modifying the stress intensity factor K_I .

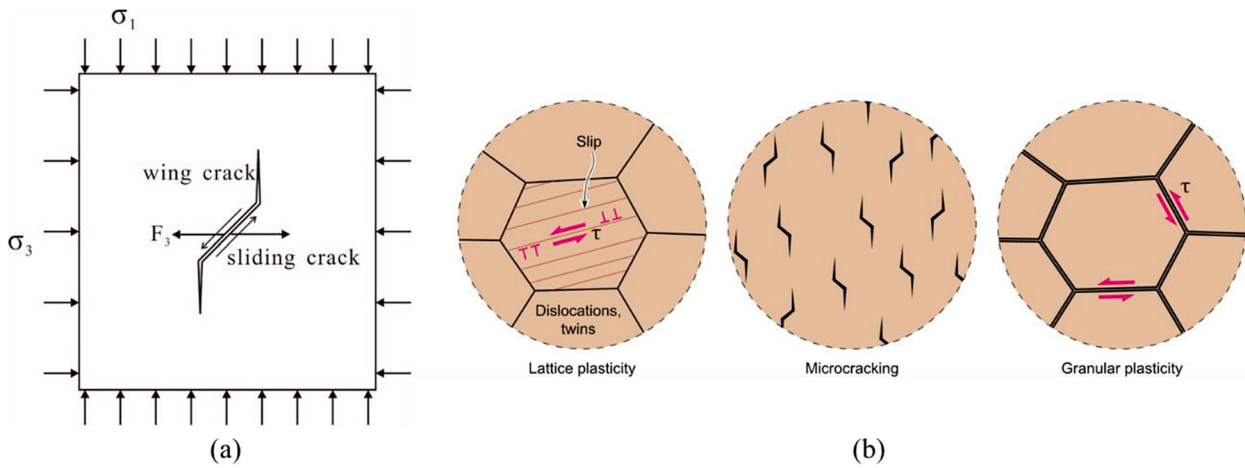


Figure 5. (a) Sketch of wing cracks nucleating from the tips of a sliding crack [77]. (b) Mechanisms of inelastic deformation and damage from Deshpande–Evans model [81].

It can be seen from Equation (1) that the critical axial stress initiating the wing cracks increases as the confining pressure is increased. As previously mentioned, the axial compressive response of a ceramic is controlled by preexisting defects and microcracks induced by external loading, with its final fracture failure and compressive strength determined by the coalescence of microcracks. As a result, increasing the confining pressure tends to prohibit the growth and propagation of wing cracks, leading to enhanced ceramic strength. If the confining pressure is sufficiently high, microcracking would not be activated. Further, premature brittle failure is prevented, and the internal stress in the crystal lattice is high enough to generate dislocation or twinning, resulting in brittle to the ductile transition of ceramic compressive behaviour (also called stress-state controlled brittle to ductile transition).

The wing-crack model laid a solid foundation for many subsequent theoretical works. For typical instance, Huang and Subhash [79] developed a dynamic model by incorporating damage rate, crack growth rate and dynamic stress intensity factor into the wing-crack model. Deshpande and Evans [80] considered the plastic deformation and crack-induced stiffness drop to characterise the inelastic deformation of ceramics under high confining pressure. They also incorporated the mechanism of granular flow for fully comminuted ceramics [81], as shown in Figure 5(b). Paliwal and Ramesh [82] presumed that the pre-existing cracks followed a certain distribution and calculated the effective stress field around a crack to imitate crack interaction. More recently, a three-dimensional (3D) model was developed by introducing tensorial damage parameter and irreversible damage strain [83], which can be used to predict the mechanical responses of ceramics under different stress states.

Existing models are mostly based on pre-existing microcracks. However, microcracks actually originate

from the pores, inclusions or other processing-induced defects. It is necessary to incorporate the formation mechanism of microcracks into the micromechanical models. Moreover, the compressive strength of ceramics is usually dispersed and should be statistically obtained, although confinement reduces the dispersity of data. Hitherto, few models take into account the effects of statistical uncertainties on the mechanical response of confined ceramics.

Phenomenological models

Phenomenological constitutive models describe empirical relationship between strength and hydrostatic pressure based on experimental results, particularly suitable for large-scale computations. In the phenomenological models, a ceramic behaves as elastic material and fails when its strength is reached. Sometimes, a notional damage process to reach the strength is adopted.

The strength of a ceramic under relatively low hydrostatic pressure can be characterised by two pressure-dependent constitutive models: the Mohr–Coulomb model and the Drucker–Prager model. The Mohr–Coulomb model describes the relationship between the shear strength τ and the hydrostatic pressure P , as:

$$\tau = \tau_0 + \alpha P \quad (2)$$

where τ_0 denotes the material strength in pure shear and α represents the proportionality constant. As for the Drucker–Prager model, the equivalent strength σ_e can be written as:

$$\sigma_e = Y_0 + \beta P \quad (3)$$

where Y_0 is the effective strength in pure shear and β is the proportionality constant. Both the Mohr–Coulomb and Drucker–Prager models are linear pressure-dependent models, but with different variables. The Drucker–Prager model has a smooth flow

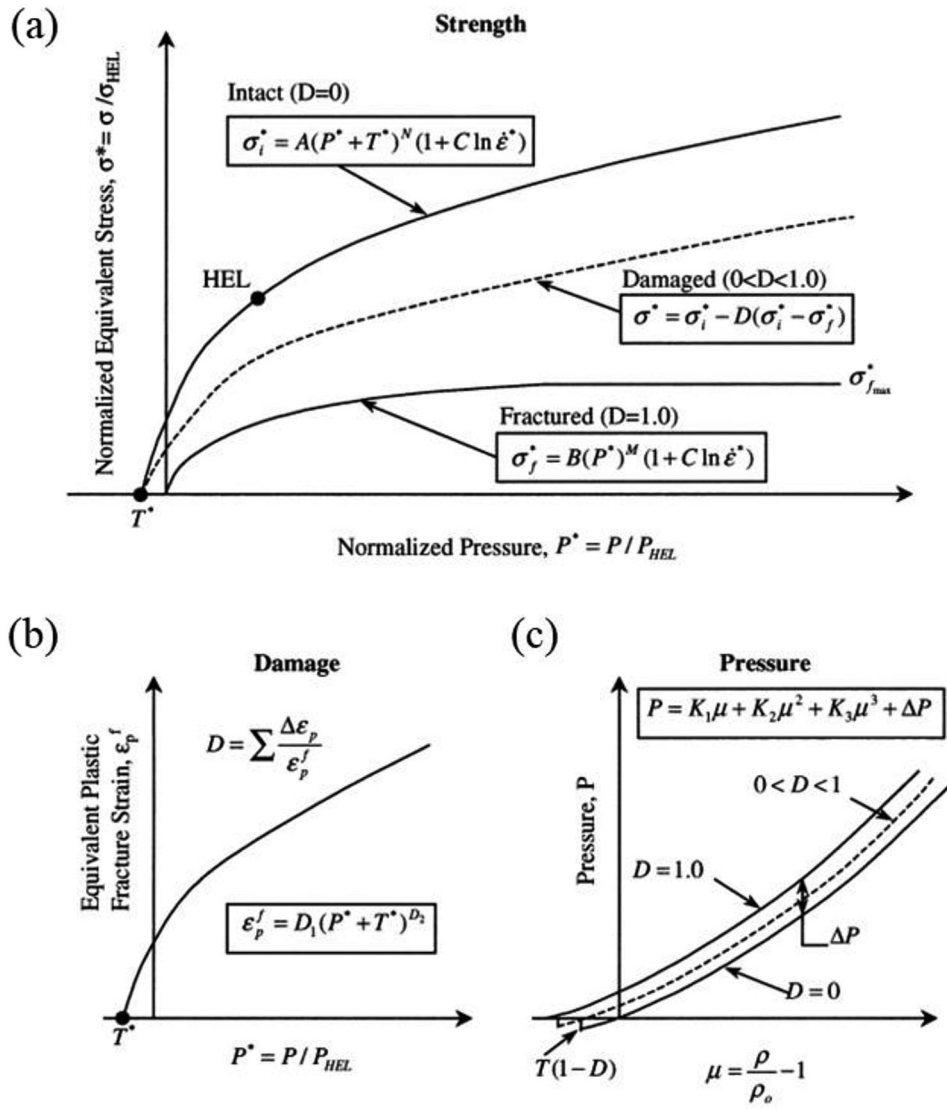


Figure 6. Descriptions of JH-2 model: (a) strength, (b) damage and (c) pressure [86].

surface without cusps, thus more suitable for computations.

The most popular phenomenological model for ceramics is the Johnson-Homquist-2 (JH-2) model, which has been implemented in commercial finite element (FE) codes and widely used to simulate projectile penetrations into ceramics [84–86]. The model includes three different types of description, i.e. strength, damage and pressure, as shown in Figure 6. In this strength-based model, the pressure dependence follows the power-law, and the rate dependence is logarithmic. The normalised intact strength σ_i^* in the JH-2 model is given by:

$$\sigma_i^* = A(P^* + T^*)^N (1 + C \ln \dot{\epsilon}^*) \quad (4)$$

After fracture, the comminuted ceramic still has a residual strength σ_f , and the normalised fracture strength σ_f^* is given by:

$$\sigma_f^* = B(P^*)^M (1 + C \ln \dot{\epsilon}^*) \quad (5)$$

It follows that the normalised strength of the damaged ceramic σ^* is:

$$\sigma^* = \sigma_i^* - D(\sigma_i^* - \sigma_f^*) \quad (6)$$

where σ_i^* , σ_f^* and σ^* are the equivalent strength normalised by the equivalent stress at the HEL (σ_{HEL}), D is the damage parameter ($0 \leq D \leq 1$), P^* is the actual hydrostatic pressure normalised by the hydrostatic pressure at HEL (P_{HEL}), and $T^* = T/P_{HEL}$, T being the maximum tensile hydrostatic pressure. The material constants A , B , C , M , N , T can be determined by fitting experimental data, but need to be recalibrated for different ceramics, which takes lots of effort. Nevertheless, it has been established that numerical simulation results obtained using the JH-2 model with proper constants agree quite well with experimental measurements.

Most recently, an extended Mohr–Coulomb model was proposed to represent the strength saturation of ceramics at high hydrostatic pressures [87], which

outperforms the JH-2 model at pressures up to the HEL. It was also suggested that, relative to the strain rate, the applied pressure plays an much more important role in ceramic constitutive behaviour, especially at pressures beyond the HEL [88].

Influence of confining pressure upon fracture and damage

Fracture modes under multiaxial compression

The fracture mode of a ceramic varies with its stress state. Under uniaxial compression without confining pressure, the mode of axial splitting is often observed. Macroscopic cracks propagate along the loading direction, with the formation of column-like ceramic fragments [89] as shown in Figure 7(a). High-speed imaging systems have been used to capture the dynamic fracture processes [90], revealing that the cracks were initiated from stress-concentrated regions, then the specimen was divided into many thin columns, and the final failure occurred as these columns collapsed, with the axial compressive stress reaching its peak.

In the presence of confining pressure, axial splitting would be inhibited. According to the wing-crack model, the flaws nucleate cracks that grow in the direction of axial compression. Because of the presence of confinement, these cracks are soon arrested. Subsequently, as the axial load is further increased,

tension cracks in a row are tend to coalesce, leading to a fault [78,92]. Under triaxial compression, a slip fault is likely to form, as shown in Figure 7(c). Chocron et al. [56] found that in confined B_4C , the diagonal fault formed along the direction with an average angle of 30° deviating from the axial loading direction. Similarly, for the glass ceramic MACOR, a conical fault was observed under the shrink-fit confinement [90]. The formation process of fault and the corresponding compressive response are summarised in Figure 8. At the beginning of compression, the ceramic specimen exhibited linear elasticity (see Figure 8(a)), as the axial stress was insufficient to cause the microcracks to nucleate or propagate. After microcracks started to initiate and propagated with the axial load, the crack density increased and the specimen became inhomogeneous, leading to decreasing moduli with increasing compressive loading (see Figure 8(b)). Subsequently, microcracks interacted and coalesced, where macroscopic cracks formed and propagated internally, as illustrated in Figure 8(c). At this time, the axial stress reached the peak, beyond which softening occurred. Once a conical fault was formed, frictional sliding between two fracture planes of the fault dominated, enabling the specimen to possess a certain load-bearing capacity and be capable of energy dissipation (see Figure 8(d)). A higher confining pressure usually resulted in a stronger effect of frictional sliding, and a greater residual strength.

Under biaxial compression, slab-like fragments could be observed with fracture surface paralleling to the free surface [91], as shown in Figure 7(b). When a compressive stress is applied in one direction, the propagation of cracks in the perpendicular direction is suppressed, forcing the cracks to propagate along the compressive direction [93]. Therefore, for biaxial compressive loading, the cracks tend to propagate along the directions of two compressive stress, i.e. in the plane parallel to the free surface, leading to the slab-like fragments.

The micro-fracture behaviour of a ceramic appears to be dependent upon both the confining pressure and strain rate [94]. For pressureless sintered AlN at low strain rates and low confining pressures, the cracks mainly propagate along grain boundaries, since the sintering additive as a second phase weakens the grain boundaries. That is to say, intergranular fracture is the dominant mechanism at low strain rates and low confining pressures. With the strain rate increased, transgranular fracture would gradually dominate, and the introduction of confining pressure would cause more failures of the second phase. However, for hot pressed AlN [95] and B_4C [91] with clean grain boundaries, the confining pressure has little effect on the fracture mechanism, and transgranular fracture remains the dominant one.

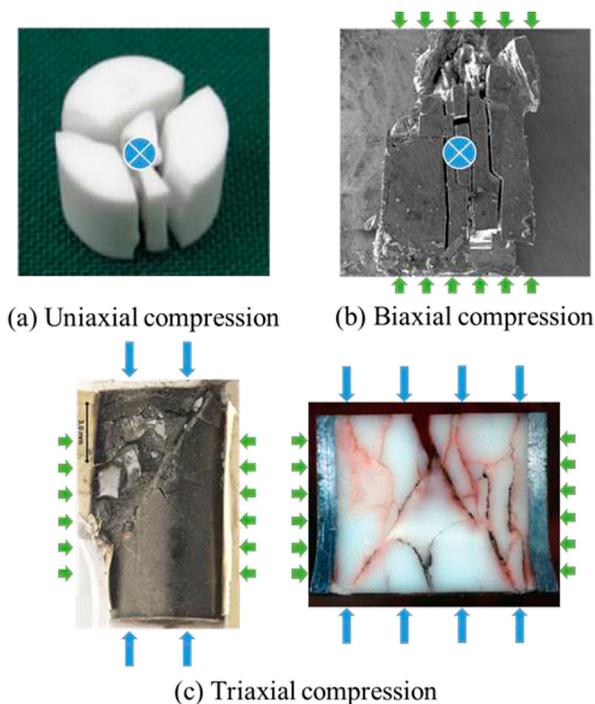


Figure 7. Fracture modes under different stress states: (a) uniaxial compression [89], (b) biaxial compression [91] and (c) triaxial compression [56,90]. Blue arrows indicate the loading direction, and green arrows refer to the direction of confining pressure.

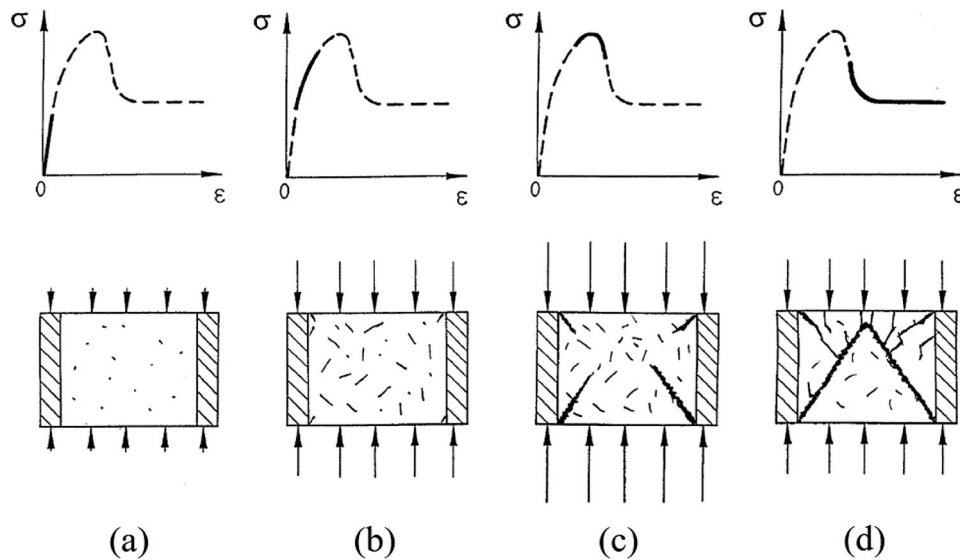


Figure 8. The axial stress–strain behaviour corresponded to the crack/damage pattern inside confined ceramic: (a) undisturbed defects, (b) initiation and propagation of microcracks, (c) formation of macrocracks and (d) frictional sliding [90].

Damage of confined ceramics impacted by projectile

Lightweight ceramic composite armour is usually consisted of a bi-layer structure: a frontal ceramic tile and a metallic or composite backing [96]. The ceramic tile with high strength/hardness can deform and erode the projectile, while the ductile backing absorbs the kinematic energies of both the projectile and ceramic fragments through deformation. Attributed to its low tensile strength and low toughness, the ceramic tile exhibits specific damage patterns after projectile impact, as shown in Figure 9. Acting as an instantaneous concentrated force, the impacting projectile would cause the tile to bend slightly, thus causing radial cracks [97] (Figure 9(a)). The ceramic region just ahead of the impact site is subjected to a huge pressure and hence fractured into fine powders [98], commonly termed as the comminuted zone. Cone cracks resulting from the shear stress start from the impact region and radiate into the backing [99]. It is noticed that the cone cracks enlarge the loading area of the back plate, resulting in more energy absorption (Figure 9(b)). Moreover, the tensile stress waves would

be reflected from the ceramic/backing interface, leading to dynamic damage in the form of spall cracks [100].

For impact testing, the confining pressure can be exerted via impedance confinement (briefly mentioned in Section 1) by inhibiting the expansion of ceramics during penetration, or by pressure confinement (also mentioned in Section 1) before penetration. However, the former is mixed with dynamic stress waves and it is difficult to obtain quantitative measurement. Thus, the pressure/prestress confinement is the preferred method for exploring the effect of confinement on ceramic damage.

The extent of damage can be reduced by lateral prestress applied on the ceramic sample. For instance, conical and radial cracks were suppressed by increasing the prestress, with the cracks diminishing or even disappearing [101]. It was also found that a ceramic specimen with prestress exhibited much less radial cracks and less cone cracks with larger conical angle [102]. In fact, the lateral prestress could eliminate the tensile component of bending stress, which suppressed the formation of radial cracks. Further, the shear strength of the ceramic could be enhanced by

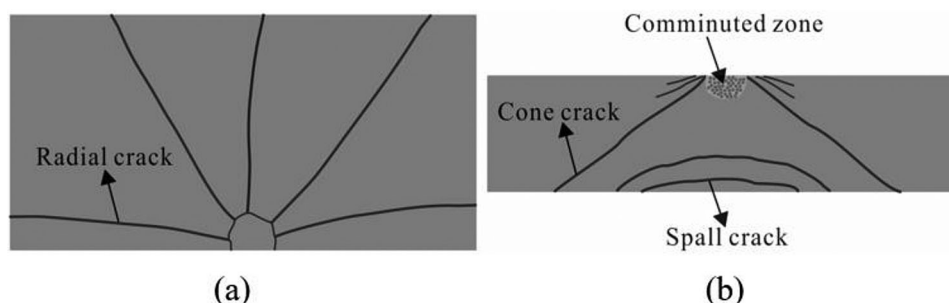


Figure 9. Sketch of crack damage on (a) impact surface and (b) cross section.

prestress, which diminished the cone cracks. However, under high-velocity penetration, the lateral prestress had little influence on damage resistance: the specimens were severely crushed so that the extent of damage was hardly assessed [102].

Systematic experiments were conducted to explore the influence of lateral prestress on the ballistic performance of alumina [103–105]. The alumina samples were supported by semi-infinite or finite thickness plates made of steel or aluminium. The number of radial cracks generated is presented Figure 10. For alumina tiles supported by steel, the number and length of radial cracks were both reduced by the presence of lateral prestress (Figure 10(a)). For alumina tiles supported by aluminium, the damage seemed to be more serious and the effects of prestress almost diminished (Figure 10(b)). Moreover, it could be found from Figure 10 that a thicker backing reduced the number of radial cracks.

Enhancement in ballistic performance

Ballistic performance enhanced by impedance confinement

Based upon Equations (4) and (5) from the phenomenological model, it is clearly that the maximum equivalent or shear strengths of intact and fully damaged ceramic are both pressure-dependent. For instance, intact Al_2O_3 and B_4C could exhibit a 5~6 fold increase in shear strength as the confining pressure increases from zero to 1 GPa [9]. As previously described in section 3.2, ceramic tiles are bound to be damaged during the penetration, and thus the strength of either the intact or damaged ceramics is important for the ballistic resistance. Due to the unique mechanical properties, the intrinsic penetration resistance provided by ceramics is dependent on both the material and the confinement configurations.

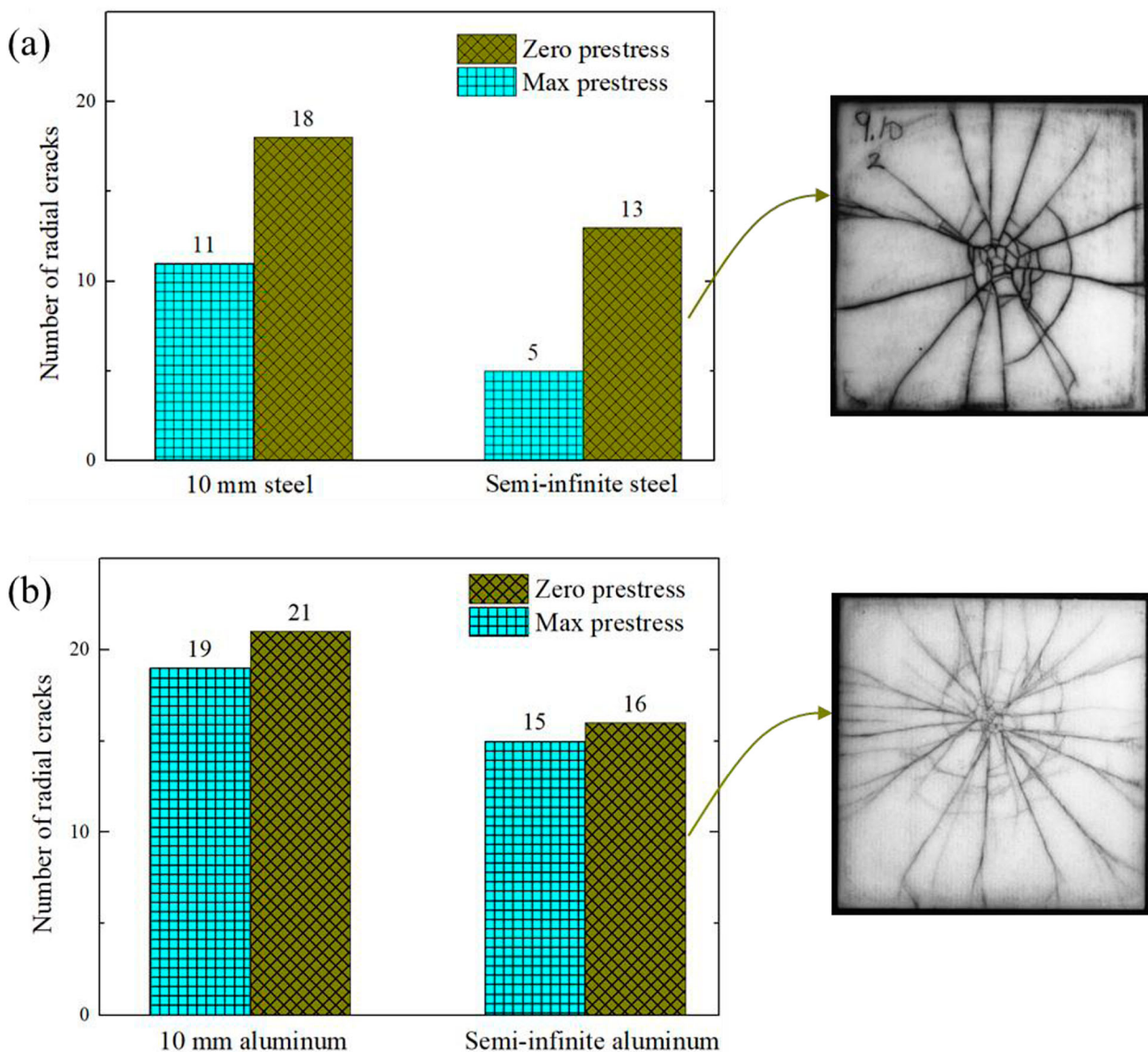


Figure 10. Number of radial cracks in ceramic tiles supported by metal plates made of (a) steel and (b) aluminium [103,104].

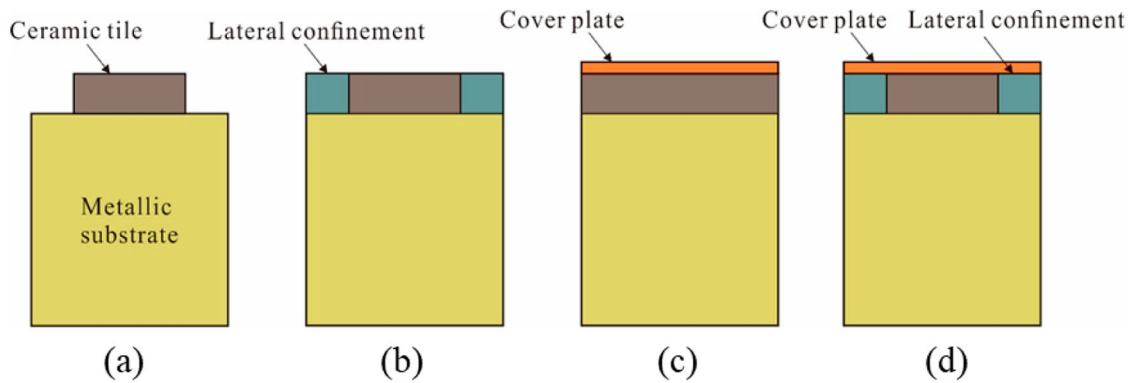


Figure 11. Sketch of target configurations (a) without confinement, (b) with lateral confinement, (c) with cover plate and (d) with cover plate and lateral confinement [106].

It has been demonstrated that confined ceramics are much more efficient in defeating the penetrator. Generally, two types of ceramic confinement have been introduced in ballistic tests, i.e. impedance confinement and pressure confinement. The former refers to the restriction on the deformation of ceramics during penetration; while the latter implies the application of prestress before penetration, which will be further discussed in subsection 4.2. For the case of impedance confinement, the ceramic could be confined by either lateral assembly (as the confinement) or cover plate with different wave impedances, as shown in Figure 11. The effects of lateral confinement and cover plate on the ballistic performance are separately discussed below.

Effect of lateral confinement

Lynch et al. [107] performed penetration tests using a tungsten-alloy long-rod projectile (LRP) against a semi-infinite Al_2O_3 target with or without lateral confinement, and found a decrease in both residual velocity and residual length of projectile for the confined target. Savio et al. [108] evaluated the ballistic performance of B_4C -based ceramic target using the standard Depth of Penetration (DOP) method against 7.62 mm armour piercing projectile. The residual penetration depth with lateral steel confinement was found to decrease by 34%, compared with that without confinement. It has been confirmed that the ratio of DOP to areal density (reflecting the ballistic efficiency) of various ceramics decreases with the increase of thickness [109]. However, for ceramic tiles with sufficient lateral confinement, the ballistic performance is relatively constant as the tile thickness is varied [110].

During the penetration process, the ceramic is usually damaged by tensile stress waves reflected from the lateral free boundary, which would lead to the degeneration of strength. With lateral confinement, the tensile stress waves could be eliminated. Further, the fragments resulted from ceramic fracture are still constrained inside the lateral confinement,

which arrest the scattering movement. As a consequence, the fragments are forced to continually rub with the projectile, leading to much more serious erosion of the projectile.

Doyoyo [34] revealed the important role of confinement impedance on the failure kinetics of ceramics subjected to impact loading. Penetration experiments with thick borosilicate targets under different lateral confinements (made of polycarbonate, aluminium and steel) showed that: the penetration depth was largest for unconfined borosilicate and smallest for aluminium-confined borosilicate; the steel-confined borosilicate was inferior to aluminium-confined borosilicate in terms of penetration resistance. However, alternative experiments by Savio et al. [108] indicated that steel-confined B_4C performed better than aluminium-confined B_4C . The difference of the two results could be interpreted by the mismatch of wave impedance, as listed in Table 3. The wave impedance mismatch between borosilicate and aluminium is the smallest, and same for the case of B_4C and steel. The lateral confinement with wave impedance close to that of ceramic target tends to have the superior performance. This is because that the small mismatch of wave impedance allows the stress waves to be transmitted to lateral confinement with little reflection to the ceramic target. Therefore, the ceramic would suffer less damage and exhibit higher penetration resistance.

Lateral confinement is generally applied at the lateral boundary of the ceramic and could be treated as a constrained boundary condition. However, this type of boundary condition could be ignored when the lateral size of the ceramic is sufficiently large [111]. Yehuda et al. [112] found that the enhancement effect of lateral confinement was significant only when the diameter ratio of ceramic to projectile was below 15. The effect of lateral confinement was negligible at impact velocities greater than 3.5 km s^{-1} [113], implying that hypervelocity penetration was dominated by local inertial properties, rather than material strength or confinement.

Table 3. Wave impedances of selected materials.

Material	Steel	Aluminium	Polycarbonate	B ₄ C	Borosilicate
Longitudinal wave impedance (10 ⁶ kg·s m ⁻²)	46.0	16.7	2.5	35.2	13.5
Shear wave impedance (10 ⁶ kg·s m ⁻²)	25.0	8.4	1.1	22.2	8.3

The grain size has an intrinsic effect on the ballistic performance, while the confinement has an extrinsic effect. When the ceramic is laterally confined, experimental measurements by James [114] revealed that the ballistic performance of alumina under the depth of penetration tests was insensitive to the grain size. However, such results might be attributed to the combination of the grain size, the porosity, impurities and other microstructural characteristics. Wei et al [115] employed the micromechanical model from Deshpande and Evans [81] to explore the mechanisms of the dynamic response of polycrystalline alumina impacted at high velocity. In the model, certain parameters were controlled to investigate the influence of grain size. For lateral confined alumina, the simulations revealed that the penetration depth was almost invariant at different impact velocities as the grain size varied (Figure 12(b)), even though the damage in a larger region was observed for the coarser-grained alumina (Figure 12(c)). However, after removing confinement, the alumina with 20 μm grain size showed an inferior penetration resistance (Figure 12 (e,f)), because of the lateral splashing of the damaged particles. Due to the limited researches, the effect of grain size on the confined ceramic needs to be further confirmed. As the microstructure plays a significant role in the resistance of materials, more work is necessary to explore the intrinsic correlation between the microstructure and ballistic performance of both confined and unconfined ceramics.

Effect of cover plate

The other type of impedance confinement is the application of cover plate in front of the ceramic. Hauver et al. [116] conducted a series of DOP tests on Al₂O₃ and found that the ceramic with cover plate possessed higher penetration resistance and smaller penetration depth into the substrate. Moreover, Ning et al. [117] found that: the damage of ceramic with cover plate was initiated from the rear face as a result of the reflected tensile wave; whereas, the damage of ceramic without cover plate was initiated from the direct impact region. Therefore, the cover plate acts as a cushion and could attenuate shock waves on the ceramic, which helps to suppress the damage caused by the direct impact of projectile. In addition, the cover plate is efficient in constraining the upward scattering of pulverised ceramic debris. Using the cover plate, Sarva et al. [118] observed much greater mushrooming and more serious erosion of the projectile (Figure 13). This implies that severer abrasion between the

ceramic and projectile could be activated by the cover plate.

The ballistic performance of ceramic with cover plate in the DOP tests (Figure 11(c)) may be quantified by the differential efficiency factor Δe_c [106], as:

$$\Delta e_c = \frac{(P_\infty - P_r)\rho_r - T_{cp}\rho_{cp}}{T_c\rho_c} \quad (7)$$

where P_r is the residual penetration depth in the rear substrate, P_∞ is the reference penetration depth into the bare substrate target; T_{cp} and T_c refer to the thickness of cover plate and ceramic; and ρ_r , ρ_{cp} and ρ_c are the densities of rear substrate, cover plate and ceramic, respectively. A larger value of Δe_c corresponds to a better ballistic performance of the ceramic component [119]. Anderson et al. [106] found that Δe_c depended upon the type of confinement and the impact velocity, as shown in Figure 14. It can be seen that lateral confinement and cover plate led to increased Δe_c . Besides, Δe_c decreased as the cover plate thickness was increased from 6.35 to 12.7 mm, implying that the ballistic performance decreased with cover thickness. However, there must be enough thickness to prevent the cover plate from bulging and hence losing the constraint effect [120], suggesting that there exists an optimal thickness for the cover plate. The results of Figure 14 also indicated that the ballistic performance should increase as the hardness (strength) of cover plate is increased.

Fibre-reinforced polymer (FRP) composites, with high specific strength and specific stiffness, have great potential in the development of lightweight armours and individual protection [121]. Several attempts have been made to cover the ceramic with FRP. For instance, Sarva et al. [118] employed the E-glass composite as the front cover of bare Al₂O₃, with an increase of areal density by 3%, and found that the residual kinetic energy of tungsten projectile was decreased by nearly 25%. However, other experiments [122] showed that fibreglass fabrics-covered alumina exhibited more damage than bare alumina when impacted by 7.62 mm projectile, with no effect on the residual kinetic energy of the projectile [123]. Crouch et al. [124] have also found that adding an aramid composite cover to boron carbide had no effect on projectile erosion, thus no improvement on ballistic performance. Existing experimental observations are somewhat conflicting, probably attributed to inconsistent projectiles used by different researchers. More systematic investigations need to be conducted to

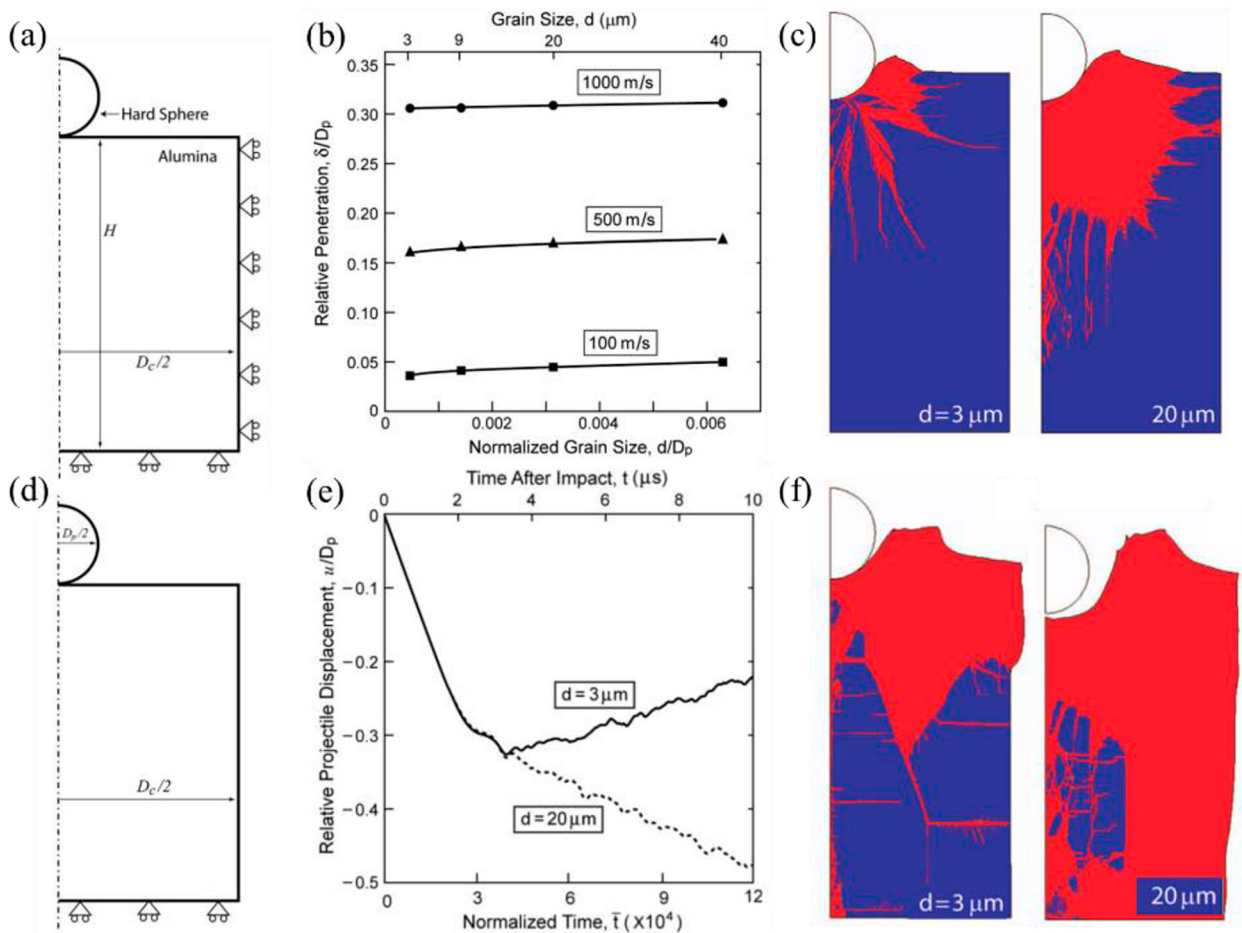


Figure 12. Effects of grain size on (b) penetration depth and (c) damage distribution for (a) the lateral confined alumina under the impact of hard sphere. For (d) unconfined alumina, (e) temporal variation of projectile displacement and (f) distributions of damage with grain sizes of 3 and 20 μm impacted at 1000 m s^{-1} are also presented [115].

explore the role of FRP composite as cover plate of ceramic targets.

Ballistic performance enhanced by pressure confinement

Exerting prestress on a ceramic has been employed as an efficient approach to improve its ballistic performance. For typical instance, DOP tests were conducted to explore the effect of lateral prestress on Al_2O_3 tiles with varying thickness [125]. The results as shown in Figure 15 indicated that the DOP decreased with the increase of prestress, and the influence of prestress on the DOP seemed to be more significant as the thickness of the ceramic tile exceeded 5 mm. A hand operated rotary apparatus was utilised to exert prestress on 20 mm thick SiC ceramic tiles [126]. It was found that the smallest DOP was obtained when the prestress was increased up to 50 MPa, but a further increase in prestress would lead to the increase of DOP. This contradicts the common belief that increasing the prestress usually leads to a better ballistic performance of ceramic. However, there may exist a transition of failure mechanism for the prestressed SiC, which needs to be further explored.

The concept of using a metal to wrap the ceramic was proposed to generate prestress using the mismatch in thermal expansion coefficient between the metal and ceramic. The metal-encapsulated ceramic was usually made by the modified investment casting [127,128]. Also, hot isostatic pressing was explored by Meyer et al. [100] to achieve a lateral prestress of 400 MPa. In these techniques, the ceramic was encapsulated by molten metal at high temperature, and subsequent solidification and shrinkage of the metal during cooling generated compressive prestress in the ceramic. The amplitude of prestress depends primarily on the material make of the encapsulation. Titanium alloy has been recommended as an ideal encapsulation material because it could provide a large prestress to the ceramic, with a small increase of area density.

Although preparation of metal-encapsulated ceramics is already achievable, they were seldom tested for ballistic resistance. Holmquist and Johnson [129] proposed a computational technique to simulate the prestress state induced by encapsulation, and numerically investigated the effect of prestress on the ballistic performance of thin ceramic targets. For a ceramic without prestress (Figure 16(a)), a cone crack occurred

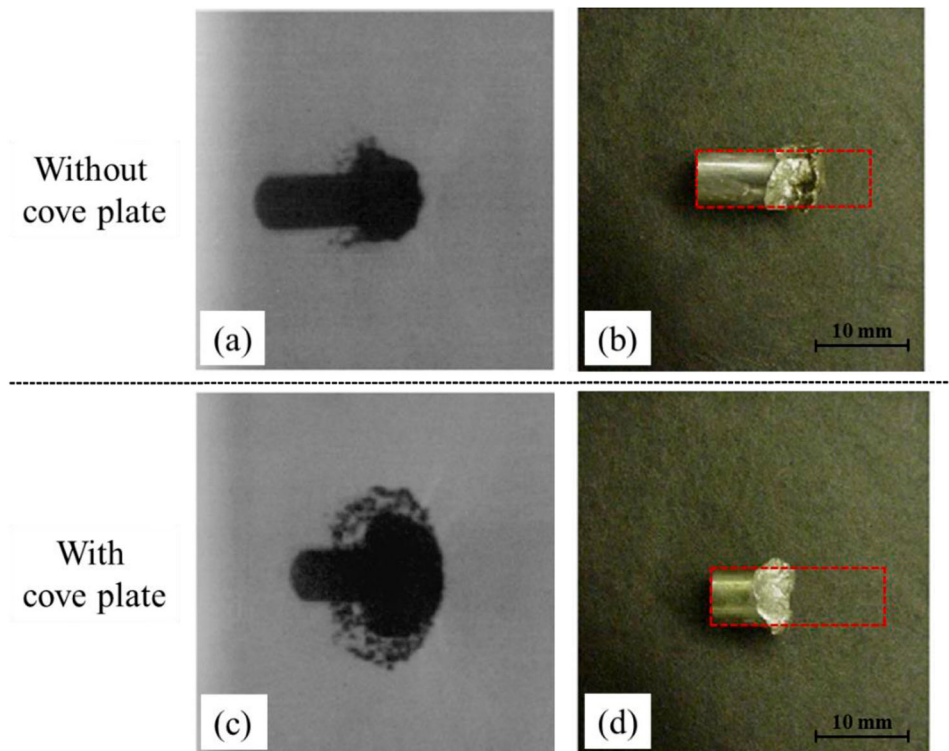


Figure 13. Mushrooming and erosion of projectile for bare Al_2O_3 tile and Al_2O_3 tile with cover plate [118]. The flat-ended projectile adopted was made of tungsten heavy alloy, with a diameter of 6 mm, a length of 19.8 mm and a mass of 10.68 g. Images (a) and (c) were taken at 8 μs , and images (b) and (d) were taken after the impact, where the shape of intact projectile was depicted in dotted line.

at 10 μs , and tensile damage at its rear interface became more serious at 20 μs , with most of the ceramic underneath the projectile fracturing. Whereas, the encapsulated ceramic with large prestress exhibited less damage (Figure 16(b)): the cone crack was prevented and premature tensile failure at the rear interface was reduced. As a result, the residual velocity and residual mass of the projectile were reduced by 30 and 10%, respectively.

Most recently, the ballistic performance of bi-layer ceramic armours was explored with the lateral

prestress exerted by a shrink-fit steel sleeve [130]. The results shown in Figure 17 indicated that the prestress efficiently improved the ballistic performance, more pronounced for larger prestress levels. It was mainly attributed to the interaction between the ceramic and projectile, which dissipated more kinetic energy via deformation and erosion of the projectile.

The strengthening mechanisms of prestress for enhanced ballistic resistance may be summarised as:

- (1) With stress-state controlled compressive strength, a ceramic would exhibit ductile deformation

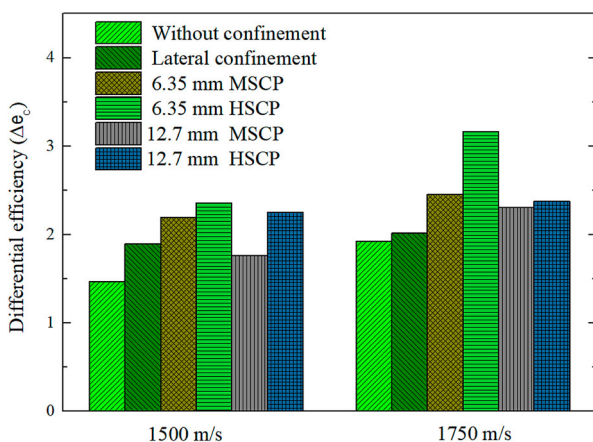


Figure 14. Differential efficiency factors of Al_2O_3 under different confinement conditions and impact velocities [106]. Ceramics with mild steel cover plate (MSCP) or hard steel cover plate (HSCP) were confined by a lateral steel surround.

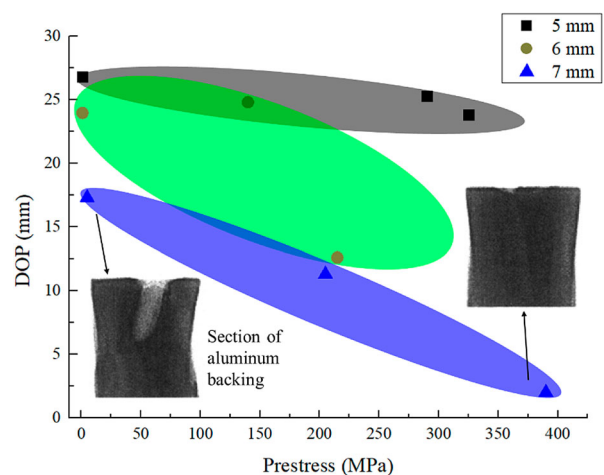


Figure 15. Effect of prestress on depth of penetration (DOP) for Al_2O_3 tiles with different thickness [125].

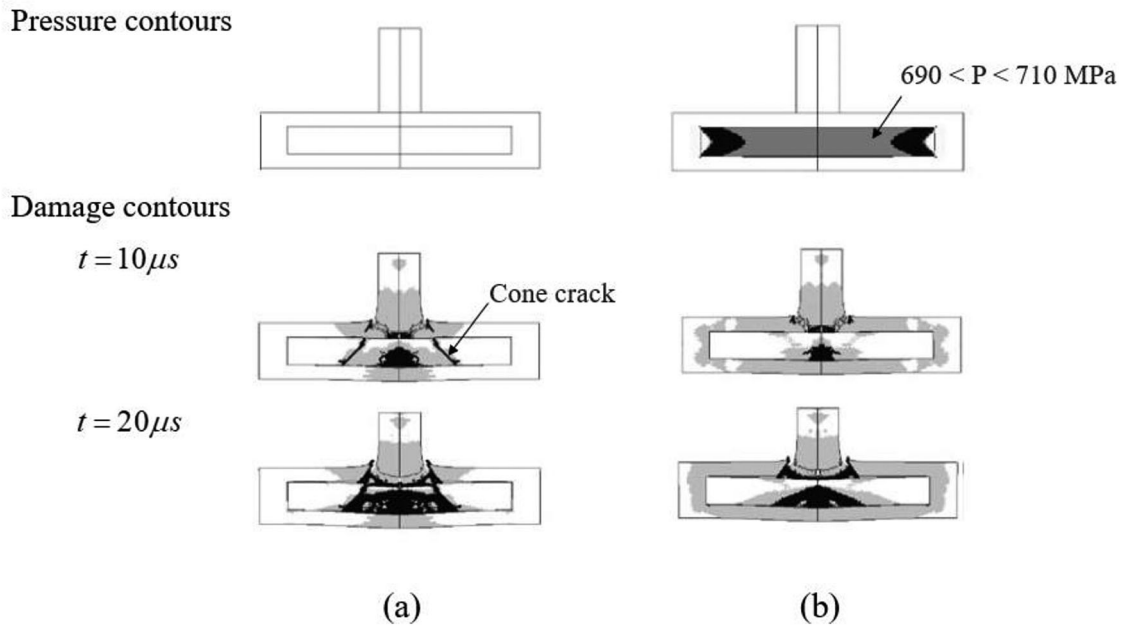


Figure 16. Computational results of target (a) without prestress and (b) with prestress [129]. In damage contours, grey represents *Partial Damage*, and black represents *Complete Failure*.

under high hydrostatic pressure. By exerting compressive prestress on the ceramic, its strength and ductility are both increased, and the initiation and propagation of cracks are suppressed, resulting in significant reduction in damage.

- (2) Tensile stress in the ceramic initiated from the boundary can be reduced or even eliminated by large prestressing, and thus the cracks induced by tensile stress wave are prohibited. Moreover, the superiority of high compressive strength of the ceramic can be fully utilised.
- (3) Compared with impedance confinement, pressure confinement can prevent the movement of ceramic fragments and further enhance the interaction between the ceramic and projectile, causing much more serious erosion of the projectile.

Effects of confinement on interface defeat and dwell

Ceramic dwell and interface defeat are two important phenomena of ceramic armours under the impact of long rod projectile [131–134]: Ceramic dwell occurs when part of the projectile erodes at the ceramic surface and flows out radially on the target surface (Figure 18); if the projectile is completely eroded at the ceramic surface, it is called as the interface defeat. When the impact velocity is below a lower threshold value, also called as the *transition velocity*, the interface defeat can be observed without penetration into the ceramic. As the impact velocity is increased, ceramic dwell occurs and lasts shortly, and subsequently the

projectile penetrates into the ceramic. Comparatively, when the impact velocity exceeds an upper threshold value, the projectile will directly penetrate into the ceramic without dwell.

Lateral confinement and prestressing are usually applied together on the ceramic to achieve interface defeat under higher velocity impact [135–139]. Andersson et al. [140] performed experiments to compare the transition velocities of unconfined SiC and prestressed SiC, and an increase of the transition velocity from 1027 to 1549 m s⁻¹ was observed for the latter case. Chi et al. [136] proposed a numerical technique to simulate interface defeat in confined ceramic targets with prestressing, and indicated that the change in transition velocity is attributed to prestress-induced increase of failure pressure. Lundberg et al. [141] developed a quasi-static theoretical model to predict the influence of lateral prestress on transition velocity, and a set of impact experiments were performed to determine the transition velocity for ceramic targets with four different prestress levels, as shown in Figure 19. It was shown that the experimentally measured improvement of transition velocity by prestress was stronger than that predicted theoretically, which might be caused by dynamic effects ignored by the theory. However, further increasing the prestress in experiments did not improve the transition velocity, with a maximum value of 1500 m s⁻¹.

The influence of cover plate on interface defeat and dwell was also explored. Although it was demonstrated that the transition velocity of SiC can be increased from 800 to 1500 m s⁻¹ by using the cover plate [142], there is still controversy concerning the material make of the cover plate. Experiments

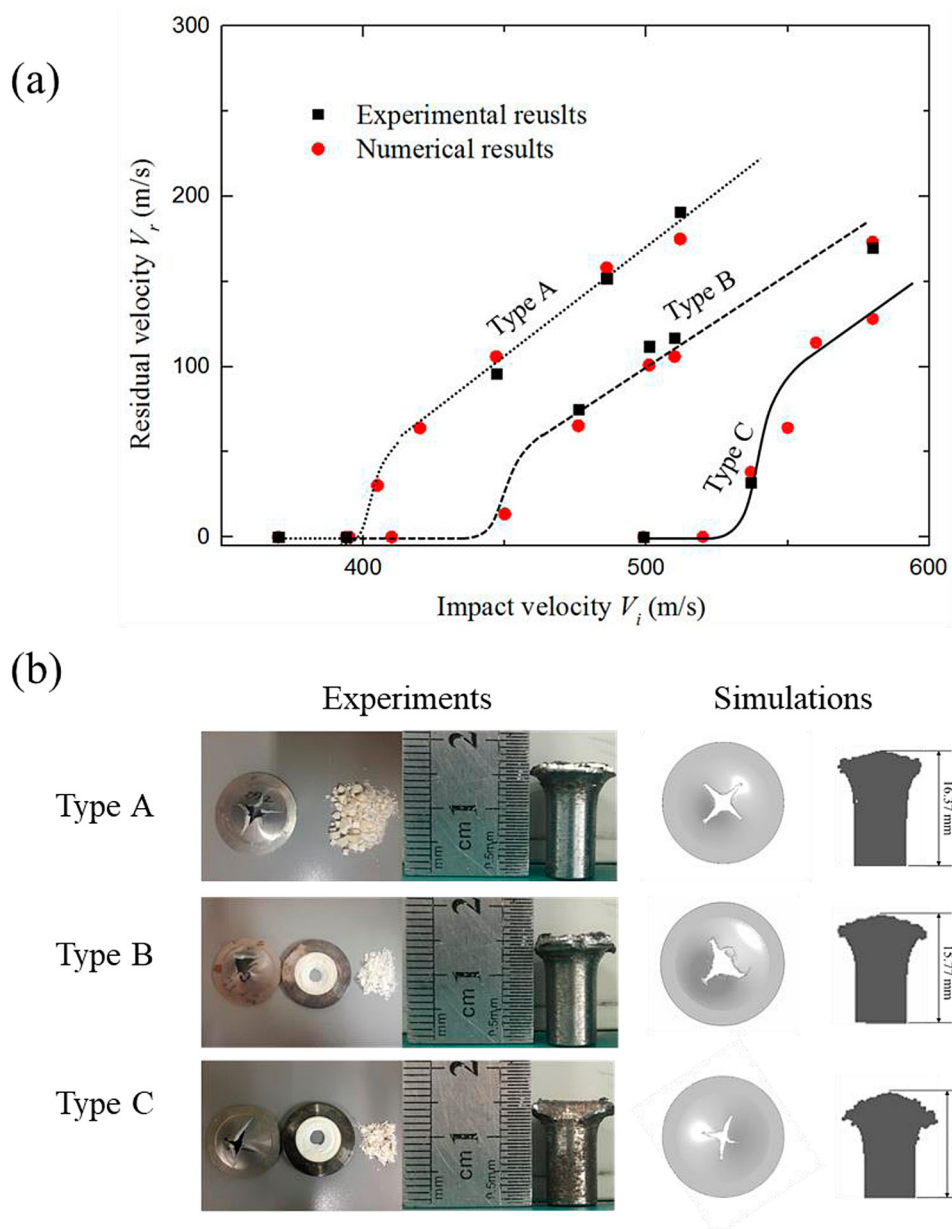


Figure 17. (a) Residual velocity versus impact velocity at different prestress levels and (b) failure modes of target plates and erosion degree of projectiles after perforation [130]. Type A – target without sleeve confinement (no prestress), Type B – target with prestress of 125 MPa, Type C – target with prestress of 274 MPa.

indicated that the thick cover plate made of steel with high hardness was quite efficient for generating interface defeat [135], whereas others showed that a thin

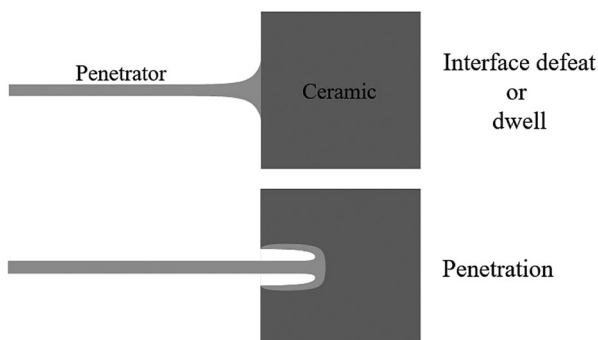


Figure 18 Schematic illustration of interface defeat, dwell and penetration.

cover plate made of the same steel had no effect on dwell and penetration [143]. In addition, a softer copper cover plate increased the transition velocity [134,142]. Therefore, it is of great worthiness to explore the role of cover material on interface defeat and dwell through systematic simulations and experiments.

The effect of confinement on interface defeat and dwell has been extensively analysed using phenomenological models of ceramics such as the Johnson and Holmquist (JH) model [129,136,142]. The model was successful in predicting key phenomena including the transition velocity and depth of penetration, and indicated that dwell ends when a critical level of ceramic damage was reached. However, these phenomenological models did not incorporate any

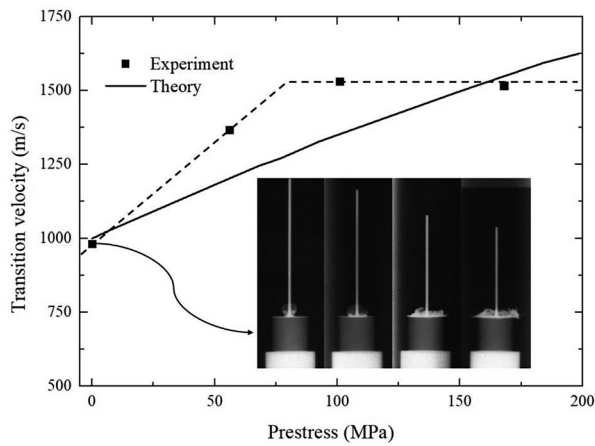


Figure 19. Transition velocity versus prestress, with X-ray images at impact velocity slightly below the transition velocity of non-prestressed silicon carbide [141].

microstructural characteristic (e.g. grain size) or other material properties (e.g. toughness and hardness), and provided little information for the making of ballistic ceramics.

The micromechanical model developed by Deshpande and Evans [81] (as described in section 2.3 and Figure 5(b)) has been implemented in the commercial software ABAQUS through a user-defined material subroutine to investigate the penetration

response of confined targets [23]. The alumina ceramic was encased by the lateral confinement, the cover and the back plate, impacted by a tungsten long rod, as shown in Figure 20(a). The influence of uniaxial yield strength (σ_Y , approximately one-third of the Vickers hardness) and toughness (K_{IC}) on the transition velocity was analysed, with the results plotted in Figure 20(b). For ceramic with low strength, the toughness had a negligible influence on the transition velocity. While at high strength, the effect of toughness became significant. The results implied that increasing the strength is a more efficient way to improve the ballistic performance for the ceramics with low strength (e.g. Corbit-98 Alumina with yield strength of 5.75 GPa and toughness of $3 \text{ MPa}\cdot\text{m}^{1/2}$). Therefore, a higher strength rather than toughness should be considered for the preparation process of these ceramics. Meanwhile, the strength of ceramic is highly dependent on the quality of precursor powder (particle size, impurity, etc.) and the sintering processing (sintering time, aid, temperature, etc.) [144,145]. Differently, for ceramics with high strength (larger than 10 GPa), it is more significant to improve fracture toughness against penetration. Approaches developed to improve the fracture toughness include the addition of fibres, second phases and microcracks [146]. Generally, high strength and toughness cannot

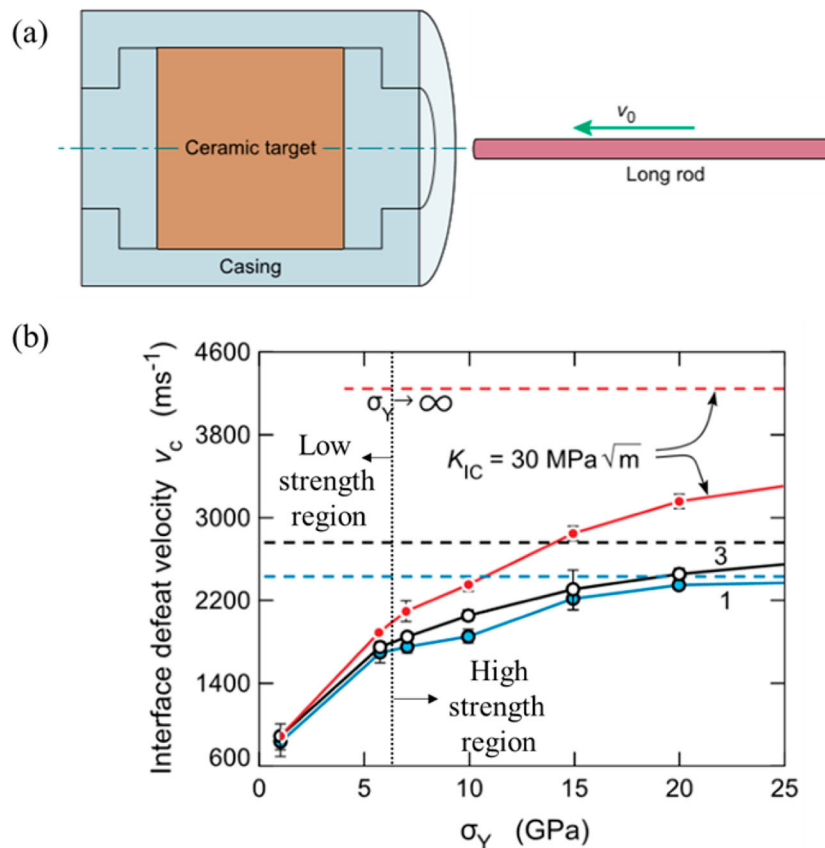


Figure 20. (a) Numerical model and (b) predictions of the influence of yield strength and toughness on the transition velocity [23]. Results are shown for three values of K_{IC} (e.g. 1, 3 and $30 \text{ MPa}\cdot\text{m}^{1/2}$) with the asymptotic values of transition velocity in the limit $\sigma_Y \rightarrow \infty$.

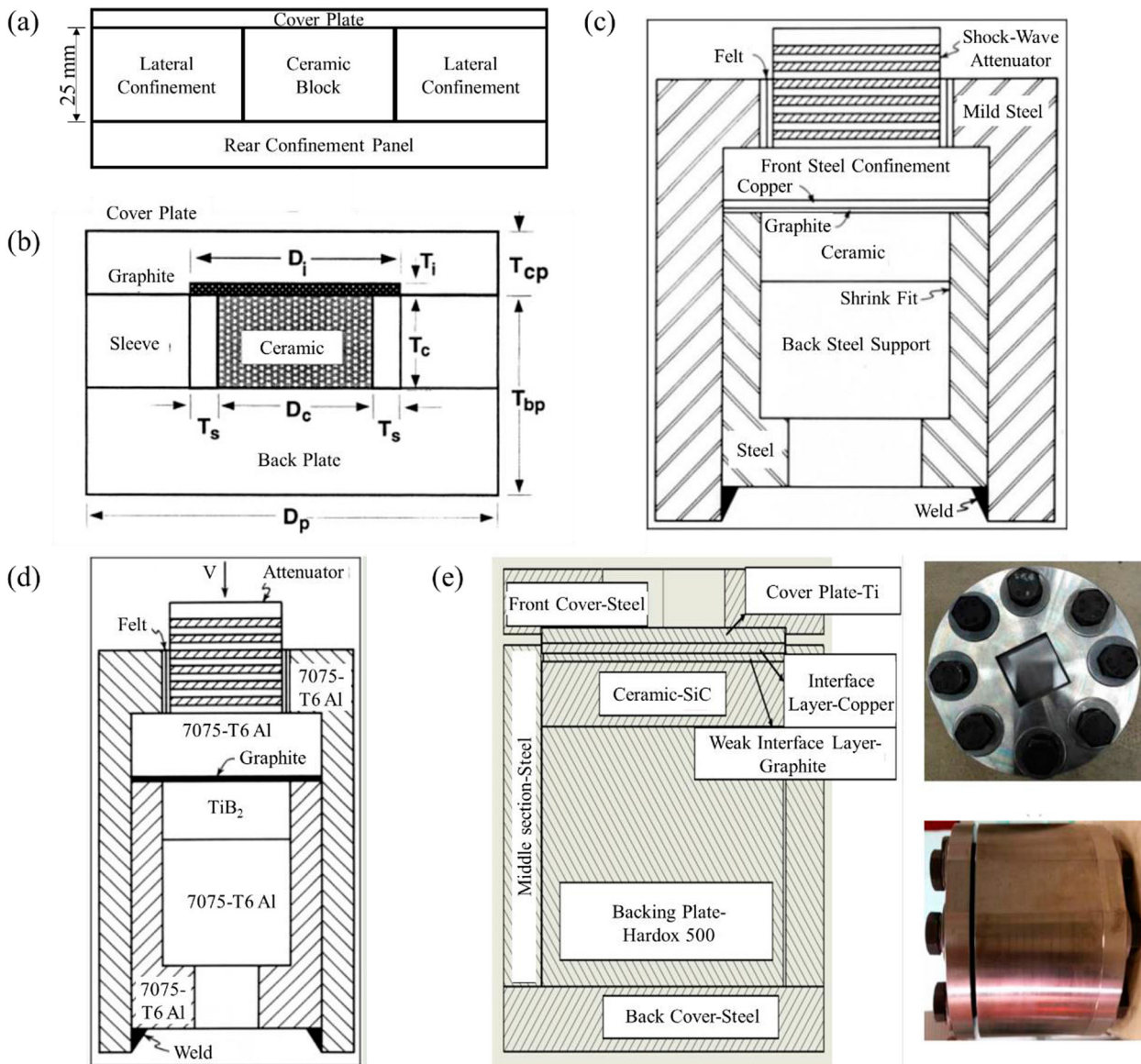


Figure 21. Schematic of different confined ceramic target configurations [126,135,148,149]. Detailed interpretation can be referred to the text.

be achieved simultaneously, and the increase in toughness may be accompanied by a decrease in strength [147]. According to Figure 20(b), it is necessary to balance the toughness and strength on the improvement of the ballistic resistance.

Application potential as composite armours

Ceramic materials have been extensively used in two types of composite armour systems. One type is a heavy armour system, commonly seen in tanks or warships, which is designed to resist the projectiles with hyper velocity and huge kinetic energy. In such heavy armour system, thick or multilayer ceramic plates are usually used. The other type consists of a thin ceramic plate (less than 15 mm) with a ductile substrate as the back cover, commonly seen in body armours and aircraft or light vehicle protection

systems, and is primarily used for defeating projectiles from light weapons and machine guns.

The ceramics employed in the heavy armour systems are commonly confined to obtain the enhanced ballistic performance, defeating the threats from the powerful anti-armours. Over the past decades, several types of confined ceramic targets have been proposed as composite armour system, as shown in Figure 19. The simplest configuration composes of steel cover plate, lateral confinement, rear confinement panel and the imbedded ceramic block [143,148] (Figure 21(a)). Improvements have been made based upon this configuration. Espinosa et al. [135] machined the bottom of cover plate to accept a graphite disk, and shrank the ceramic disk to fit in a steel ring, which further shrank into another steel ring with a larger diameter (Figure 21(b)). The target was assembled by using bolts and the rigidity was enhanced by welding at the interfaces. As a result, this target completely

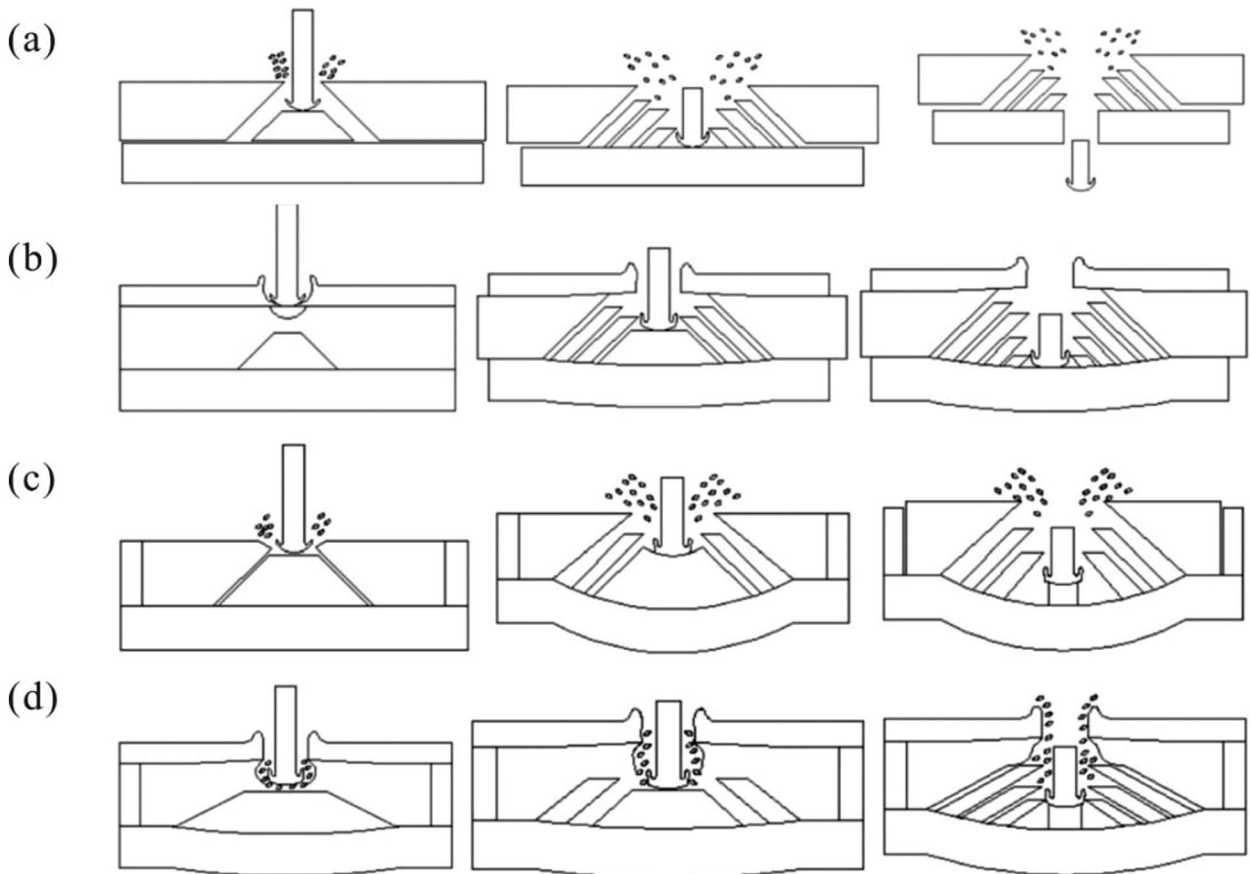


Figure 22. Penetration processes of ceramic composite armours (a) without confinement, (b) with cover plate, (c) with lateral confinement and (d) with cover plate and lateral confinement [150].

defeated the long rod bullet made of Tungsten alloy with a velocity of 1.5 km s^{-1} . The heavy target configuration proposed by Hauver et al. [149] added a shock wave attenuator block on the top, and a copper layer was placed in the interface between the cover plate and graphite (Figure 21(c)). Similarly, the shrink-fit method was used for the assembly of the ceramic. By replacing the steel with 7075-T6 Al, the weight of the target could be significantly reduced (Figure 21(d)). Serjouei et al. [126] proposed a hybrid ceramic armour design by using high-performance materials, including Ti-6Al-4V, Hardox 500 armour steel and SiC ceramic (Figure 21(e)). The target successfully defeated the long rod projectiles with kinetic energy of 50.5 kJ at the ceramic surface. This design can be applied for multiple shots and it is easier to remove the damaged ceramic and other layers.

For the lightweight armour system with thin ceramic and substrate, some applications of confinement have been achieved. Tan et al. [150] applied different confinements to bilayer alumina/steel armours and conducted ballistic tests. Figure 22 presented the observed penetration processes for different types of targets. Impacted by the same projectile, the target without confinement was perforated (see Figure 22 (a)), while the targets with cover plate or lateral confinement survived, with plastic bulging in the

steel backing (see Figure 22(b,c,d)). Moreover, by using the shrink fit technique, a bi-layer composite armour with prestressed ceramic was proposed [130]. The experimental and numerical results (see Figure 17(a)) had all shown the ballistic limit velocity could be increased by 25% at the same thickness, when compared to the traditional bi-layer ceramic armour.

Another application of confined ceramics is in sandwich structures. Sandwich plates with lattice truss cores also attracted great attention for multifunctional hybrid design due to their periodic interstices [151–153]. Ceramic prisms have been inserted into the interstices of the lattice core to improve the ballistic resistance of sandwich plates [154–157]. In such hybrid structures, the inserted ceramics are fully constrained by metallic lattices. Corrugated metallic lattices were found to impede the continuous propagation of cracks in the discrete ceramic prisms and prevent the nucleation of new cracks in adjacent prisms, thereby limiting the damage within only three unit cells (Figure 23(a)) [158]. Moreover, decreasing the number of inclined lattices would result in a decreased residual velocity but increased damage area in the ceramic (Figure 23(b)) [159]. This implies that there exists an optimal design of mass efficiencies for a specified threat level, making a trade-off for the resistance requirement of both multi-hit and single impact.

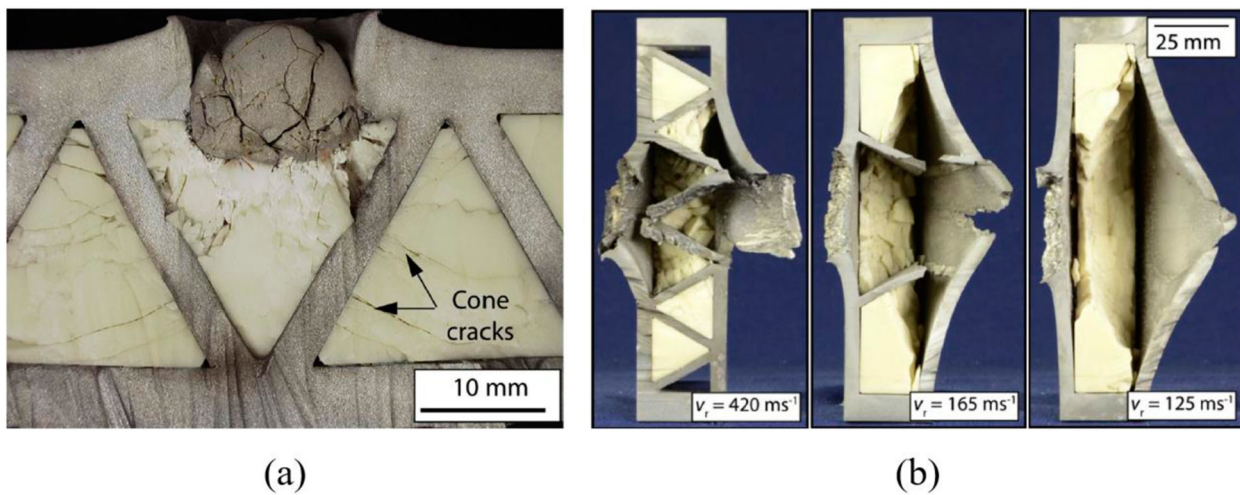


Figure 23. (a) Damage of ceramic prisms in all-metallic lattice-cored sandwich panels after impact at 656 m s^{-1} and (b) cross sections of samples with different cores tested at an impact velocity of 1600 m s^{-1} , with residual velocity shown on lower right [159].

However, in practice, application of confinement inevitably increases the total mass of the armour system, which may be a conflict with the optimisation to achieve best performance at the minimum weight. Results from numerical simulations [126,160] indicated that the bilayer ceramic/metal armour outperformed the trilayer metal/ceramic/metal armour in term of ballistic resistance. Note that, in the simulations, the influence of cover plate on the ballistic performance might be underestimated since the ejecting of ceramic fragments was not effectively simulated. The numerical results need to be confirmed by experiments. Moreover, the mass efficiency of lateral confinement is seldom evaluated, and deserves more attention.

Concluding remarks

The effects of confinement on the compressive performance and ballistic response of ceramics are systematically reviewed. Confining pressure inhibits nucleation and propagation of cracks, leading to enhanced ceramic strength under compressive loading. Further, ductile deformation could occur if the confining pressure is sufficiently high to prevent premature brittle failure. The fracture mode of a ceramic under uniaxial compression is also changed by confining pressure, from axial splitting mode to slip fault or slab-like mode. The ballistic performance of ceramics can also be enhanced by confinements. Impedance confinement including lateral assembly and cover plate can arrest the scattering movement of ceramic fragments and force the fragments to rub against the penetrating projectile. Pressure confinement can further increase ceramic strength and prohibit cracks induced by tensile stress waves, leading to a significant reduction in damage and great improvement in

ballistic resistance. In addition, confinement plays an important role in interface defeat and dwell, which is conducive to defeat long rod projectile on the ceramic surface.

Even though large efforts have been devoted to revealing the compressive and ballistic performances of confined ceramics, challenges still remain in the exploration of underlying physical mechanisms and practical applications. Further efforts in several directions deserve to be done, as summarised below:

First, a deeper understanding of the mechanical properties of armour ceramics under high confining pressure is required. Although ductile deformation has been directly observed in experiments with low-strength ceramics such as BeO and AlN, such phenomenon in ballistic ceramic rarely occurs, due to insufficient confining pressure. There is need for advanced confinement technique to provide controllable pressure up to 5 GPa, which enables revealing the relationship between ceramic strength and hydrostatic pressure at a certain strain rate. To date, focus has been mainly placed upon the compressive behaviours of intact ceramics, and much less work was conducted on pre-damaged ceramics or ceramic fragments. Moreover, it is necessary to further improve existing micromechanical models by incorporating the formation mechanism of microcracks and considering statistical uncertainties on the mechanical response of confined ceramics.

Second, reducing the weight of actual armours requires further optimisation of the confinement system. Attention should not only be paid on the ballistic enhancement effects of impedance confinement and pressure confinement, but also on the mass efficiency. The material makes and geometrical dimensions of the confinement system should also be optimised. As there are controversies on cover plate about its mass

efficiency, thickness and hardness, more systematic investigations are necessitated to provide guidance for practical application of the cover plate. The metal-encapsulated prestressed ceramic strategy seems to be promising to achieve the best performance at minimal weight, demonstrating great potential for actual armour applications. Besides, confinement effects on interface defeat and dwell have been explored only in laboratories at relatively small scale.

Finally, the relationship between the multi-axial compressive response of a ceramic and its ballistic performance should be explored. Because of the complexity of ballistic problems, it is difficult to extrapolate from ceramic performance obtained at ordinary laboratory conditions (e.g. hardness, fracture toughness, tensile strength) to that at impact conditions [161]. Since the ceramic region just ahead of an impacting projectile is in the state of multiaxial compression, the critical mechanical parameters depend on the complicated stress state for confined ceramics under impacting [9]. Such a link is helpful for building theoretical frameworks for modelling the ballistic performance of confined ceramics and selecting ceramic materials for high-performance armour applications.

Acknowledgements

The authors gratefully acknowledge financial support by the National Natural Science Foundation of China (11802221, 11972185 and 51875441), the National Key R&D Program of China (2018YFB1106400), Zhejiang Provincial Natural Science Foundation of China (LGG18A020001), the Natural Science Fund Project in Jiangsu Province of China (BK20190392), and the Open Fund of the State Key Laboratory of Mechanics and Control of Mechanical Structures (MCMS-I-0219K01 and MCMS-E0219K02).

Disclosure statement

No potential conflict of interest was reported by the author(s).

Funding

The authors gratefully acknowledge financial support by the National Natural Science Foundation of China [grant number 11802221, 11972185, 12072250 and 51875441], the National Key R&D Program of China [2018YFB1106400], Zhejiang Provincial Natural Science Foundation of China [LGG18A020001], the Natural Science Fund Project in Jiangsu Province of China [BK20190392], and the Open Fund of the State Key Laboratory of Mechanics and Control of Mechanical Structures [MCMS-I-0219K01 and MCMS-E0219K02].

References

- [1] Anselmi-Tamburini U, Maglia F, Chiodelli G, et al. Enhanced low-temperature protonic conductivity in fully dense nanometric cubic zirconia. *Appl Phys Lett*. 2006;89(16):805.
- [2] Dorey RA, Rocks SA, Dauchy F, et al. Integrating functional ceramics into microsystems. *J Eur Ceram Soc*. 2008;28(7):1397–1403.
- [3] Yang J, Hu Y. Mechanics of electroelastic bodies under biasing fields. *Appl Mech Rev*. 2004;57(3):173–189.
- [4] Joschek S, Nies B, Krotz R, et al. Chemical and physicochemical characterization of porous hydroxapatite ceramics made of Natural bone. *Biomaterials*. 2000;21(16):1645–1658.
- [5] Thümmler F. Engineering ceramics. *J Eur Ceram Soc*. 1990;6(3):139–151.
- [6] Senthil Kumar A, Raja Durai A, Sornakumar T. Wear behaviour of alumina based ceramic cutting tools on machining steels. *Tribol Int*. 2006;39(3):191–197.
- [7] Belmonte M. Advanced ceramic materials for high temperature applications. *Adv Eng Mater*. 2006;8(8):693–703.
- [8] Gama BA, Bogetti TA, Fink BK, et al. Aluminum foam integral armor: a new dimension in armor design. *Compos Struct*. 2001;52(3):381–395.
- [9] Wilkins ML, Cline CF, Honodel CA. Fourth progress report of light armor program, UCRL-50694, Lawrence Livermore National Laboratory, Livermore, CA. 1969.
- [10] Gooch WA. An overview of ceramic armor applications. Hawaii. International Conference on Advanced Ceramics and Glass. 2001.
- [11] Madhu V, Ramanjaneyulu K, Balakrishna Bhat T, et al. An experimental study of penetration resistance of ceramic armour subjected to projectile impact. *Int J Impact Eng*. 2005;32(1–4):337–350.
- [12] Lundberg P, Westerling L, Lundberg B. Influence of scale on the penetration of tungsten rods into steel-backed alumina targets. *Int J Impact Eng*. 1996;18(4):403–416.
- [13] Schuster BE, Aydelotte BB, Leavy RB, et al. Concurrent velocimetry and flash X-ray characterization of impact and penetration in an armor ceramic. *Proc Eng*. 2015;103:553–560.
- [14] Jiusti J, Kammer EH, Neckel L, et al. Ballistic performance of Al₂O₃ mosaic armors with gap-filling materials. *Ceram Int*. 2017;43(2):2697–2704.
- [15] Cottrell MG, Yu J, Owen DRJ. The adaptive and erosive numerical modelling of confined boron carbide subjected to large-scale dynamic loadings with element conversion to undeformable meshless particles. *Int J Impact Eng*. 2003;28(9):1017–1035.
- [16] Fawaz Z, Zheng W, Behdian K. Numerical simulation of normal and oblique ballistic impact on ceramic composite armors. *Compos Struct*. 2004;63(3–4):387–395.
- [17] Krishnan K, Sockalingam S, Bansal S, et al. Numerical simulation of ceramic composite armor subjected to ballistic impact. *Compos Part B Eng*. 2010;41(8):583–593.
- [18] Woodward RL. A simple one-dimensional approach to modelling ceramic composite armour defeat. *Int J Impact Eng*. 1990;9(4):455–474.
- [19] Forrestal MJ, Longcope DB. Target strength of ceramic materials for high-velocity penetration. *J Appl Phys*. 1990;67(8):3669–3672.
- [20] Zaera R, Sánchez-Gálvez V. Analytical modelling of normal and oblique ballistic impact on ceramic/metal lightweight armors. *Int J Impact Eng*. 1998;21(3):133–148.

- [21] Clayton JD. Penetration resistance of armor ceramics: dimensional analysis and property correlations. *Int J Impact Eng.* 2015;85:124–131.
- [22] Feli S, Aalami Aaleagha ME, Ahmadi Z. A new analytical model of normal penetration of projectiles into the light-weight ceramic–metal targets. *Int J Impact Eng.* 2010;37(5):561–567.
- [23] Das S, Ronan W, Wadley HNG, et al. Penetration of confined ceramics targets. *Extreme Mech Lett.* 2018;18:45–57.
- [24] Feli S, Asgari MR. Finite element simulation of ceramic/composite armor under ballistic impact. *Compos Part B Eng.* 2011;42(4):771–780.
- [25] Zhang D, Wu MS, Feng R. Micromechanical investigation of heterogeneous microplasticity in ceramics deformed under high confining stresses. *Mech Mater.* 2005;37(1):95–112.
- [26] Pandolfi A, Conti S, Ortiz M. A recursive-faulting model of distributed damage in confined brittle materials. *J Mech Phys Solids.* 2006;54(9):1972–2003.
- [27] Holland CC, McMeeking RM. The influence of mechanical and microstructural properties on the rate-dependent fracture strength of ceramics in uniaxial compression. *Int J Impact Eng.* 2015;81:34–49.
- [28] Lee S, Ravichandran G. Crack initiation in brittle solids under multiaxial compression. *Eng Fract Mech.* 2003;70(13):1645–1658.
- [29] Gamble EA, Compton BG, Deshpande VS, et al. Damage development in an armor ceramic under quasi-static indentation. *J Am Ceram Soc.* 2011;94:s215–s225.
- [30] Sternberg J. Material properties determining the resistance of ceramics to high velocity penetration. *J Appl Phys.* 1989;65(9):3417–3424.
- [31] Rozenberg Z, Yeshurun Y. The relation between ballistic efficiency and compressive strength of ceramic tiles. *Int J Impact Eng.* 1988;7(3):357–362.
- [32] Haney EJ, Subhash G. Damage mechanisms perspective on superior ballistic performance of spinel over sapphire. *Exp Mech.* 2012;53(1):31–46.
- [33] Brian R. Indentation of ceramics with spheres: a century after hertz. *J Am Ceram Soc.* 2010;81(8):1977–1994.
- [34] Doyoyo M. Experiments on the penetration of thin long-rod projectiles into thick long-cylindrical borosilicate targets under pressure-free polycarbonate, aluminum and steel confinements. *Int J Solids Struct.* 2003;40(20):5455–5475.
- [35] Gubernat A, Stobierski L, Łabaj P. Microstructure and mechanical properties of silicon carbide pressureless sintered with oxide additives. *J Eur Ceram Soc.* 2007;27(2–3):781–789.
- [36] Grabchuk BL, Kislyi PS. The sintering of technical boron carbide. *Sov Powder Metall Met Ceram.* 1974;13(8):612–616.
- [37] Bakas MP, Greenhut VA, Niesz DE, et al. Anomalous defects and dynamic failure of armor ceramics. *Int J Appl Ceram Technol.* 2004;1(3):211–218.
- [38] Flinders M, Ray D, Anderson A, et al. High-toughness silicon carbide as armor. *J Am Ceram Soc.* 2005;88(8):2217–2226.
- [39] Wereszczak AA, Lin H-T, Gilde GA. The effect of grain growth on hardness in hot-pressed silicon carbides. *J Mater Sci.* 2006;41(15):4996–5000.
- [40] Chen MW, McCauley JW, LaSalvia JC, et al. Microstructural characterization of commercial hot-pressed boron carbide ceramics. *J Am Ceram Soc.* 2005;88(7):1935–1942.
- [41] Aghajanian MK, Morgan BN, Singh JR, et al. A new family of reaction bonded ceramics for armor applications. *Ceram Trans.* 2002;134:527–539.
- [42] Karandikar PG, Evans G, Wong S, et al. A review of ceramics for armor applications. Florida. International Conference on Advanced Ceramics and Composite Materials. 2009.
- [43] Demuyneck M, Erauw J-P, Van der Biest O, et al. Densification of alumina by SPS and HP: a comparative study. *J Eur Ceram Soc.* 2012;32(9):1957–1964.
- [44] Langer J, Hoffmann MJ, Guillon O. Direct comparison between hot pressing and electric field-assisted sintering of submicron alumina. *Acta Mater.* 2009;57(18):5454–5465.
- [45] Munir ZA, Anselmi-Tamburini U, Ohyanagi M. The effect of electric field and pressure on the synthesis and consolidation of materials: a review of the spark plasma sintering method. *J Mater Sci.* 2006;41(3):763–777.
- [46] Mccuiston R, Lasalvia J, Mccauley J, et al. The possible roles of stoichiometry, microstructure, and defects on the mechanical behavior of boron carbide. Florida. International Conference on Advanced Ceramics and Composite Materials. 2008.
- [47] Lankford J, Predebon WW, Staehler JM, et al. The role of plasticity as a limiting factor in the compressive failure of high strength ceramics. *Mech Mater.* 1998;29(3–4):205–218.
- [48] Hu G, Ramesh KT, Cao B, et al. The compressive failure of aluminum nitride considered as a model advanced ceramic. *J Mech Phys Solids.* 2011;59(5):1076–1093.
- [49] Hogan JD, Farbaniec L, Mallick D, et al. Fragmentation of an advanced ceramic under ballistic impact: mechanisms and microstructure. *Int J Impact Eng.* 2017;102:47–54.
- [50] Schock RN, Heard HC, Stephens DR. Stress-strain behavior of a granodiorite and two graywackes on compression to 20 kilobars. *J Geophys Res.* 1973;78(26):5922–5941.
- [51] Heard HC, Carter NL. Experimentally induced natural intragranular flow in quartz and quartzite. *Am J Sci.* 1968;266(1):1–42.
- [52] Dannemann KA, Chocron S, Nicholls AE, et al. Compressive damage development in confined borosilicate glass. *Mater Sci Eng A.* 2008;478(1–2):340–350.
- [53] Chocron S, Walker JD, Nicholls AE, et al. Analytical model of the confined compression test used to characterize brittle materials. *J Appl Mech.* 2008;75(2):021006.
- [54] Chocron S, Anderson CE, Nicholls AE, et al. Characterization of confined intact and damaged borosilicate glass. *J Am Ceram Soc.* 2010;93(10):3390–3398.
- [55] Heard HC, Cline CF. Mechanical behaviour of polycrystalline BeO, Al₂O₃ and AlN at high pressure. *J Mater Sci.* 1980;15(8):1889–1897.
- [56] Chocron S, Anderson CE, Jr, Dannemann KA, et al. Intact and predamaged boron carbide strength under moderate confinement pressures. *J Am Ceram Soc.* 2012;95(1):350–357.
- [57] Munson DE, Lawrence RJ. Dynamic deformation of polycrystalline alumina. *J Appl Phys.* 1979;50(10):6272–6282.

- [58] Klopp RW, Shockey DA. The strength behavior of granulated silicon carbide at high strain rates and confining pressure. *J Appl Phys.* 1991;70(12):7318–7326.
- [59] Grady DE. Shock-wave compression of brittle solids. *Mech Mater.* 1998;29(3–4):181–203.
- [60] Chen MW, McCauley JW, Dandekar DP, et al. Dynamic plasticity and failure of high-purity alumina under shock loading. *Nat Mater.* 2006;5(8):614–618.
- [61] Bourne NK, Millett JCF, Chen M, et al. On the Hugoniot elastic limit in polycrystalline alumina. *J Appl Phys.* 2007;102(7):073514.
- [62] Zaretsky EB, Kanel GI. Evidence of ductile response of alumina ceramic under shock wave compression. *Appl Phys Lett.* 2002;81(7):1192–1194.
- [63] Rosenberg Z, Brar NS, Bless SJ. Dynamic high-pressure properties of AlN ceramic as determined by flyer plate impact. *J Appl Phys.* 1991;70(1):167–171.
- [64] Rosenberg Z, Yaziv D, Yeshurun Y, et al. Shear strength of shock-loaded alumina as determined with longitudinal and transverse manganin gauges. *J Appl Phys.* 1987;62(3):1120–1122.
- [65] Kipp ME, Grady DE. Shock compression and release in high-strength ceramics. Sandia Report SAND89-1461, Sandia National Laboratory, NM 87185, U.S.A. 1990.
- [66] Gama BA, Lopatnikov SL, Gillespie JW, Jr. Hopkinson bar experimental technique: a critical review. *Appl Mech Rev.* 2004;57(4):223–250.
- [67] Chen WN, Ravichandran G. Dynamic compressive failure of a glass ceramic under lateral confinement. *J Mech Phys Solids.* 1997;45(8):1303–1328.
- [68] Chen WN, Ravichandran G. Failure mode transition in ceramics under dynamic multiaxial compression. *Int J Fract.* 2000;101(1–2):141–159.
- [69] Chen WN, Ravichandran G. Static and dynamic compressive behavior of aluminum nitride under moderate confinement. *J Am Ceram Soc.* 1996;79(3):579–584.
- [70] Shafiq M, Subhash G. Dynamic deformation characteristics of zirconium diboride–silicon carbide under multi-axial confinement. *Int J Impact Eng.* 2016;91:158–169.
- [71] Shafiq M, Subhash G. A novel technique for the determination of surface biaxial stress under external confinement using Raman spectroscopy. *Exp Mech.* 2014;54(5):763–774.
- [72] Lankford J, Anderson CE, Nagy AJ, et al. Inelastic response of confined aluminium oxide under dynamic loading conditions. *J Mater Sci.* 1998;33(6):1619–1625.
- [73] Paliwal B, Ramesh KT, McCauley JW, et al. Dynamic compressive failure of AlON under controlled planar confinement. *J Am Ceram Soc.* 2008;91(11):3619–3629.
- [74] Hogan JD, Farbaniec L, Shaeffer M, et al. The effects of microstructure and confinement on the compressive fragmentation of an advanced ceramic. *J Am Ceram Soc.* 2015;98(3):902–912.
- [75] Costin LS. A microcrack model for the deformation and failure of brittle rock. *J Geophys Res Solid Earth.* 1983;88(B11):9485–9492.
- [76] Ashby MF, Hallam SD. The failure of brittle solids containing small cracks under compressive stress states. *Acta Metall.* 1986;34(3):497–510.
- [77] Ashby MF, Sammis CG. The damage mechanics of brittle solids in compression. *Pure Appl Geophys.* 1990;133(3):489–521.
- [78] Horii H, Nemat-Nasser S. Brittle failure in compression: splitting, faulting and brittle-ductile transition. *Phil Trans Roy Soc A Math Phys Eng Sci.* 1986;319(1549):337–374.
- [79] Huang C, Subhash G. Influence of lateral confinement on dynamic damage evolution during uniaxial compressive response of brittle solids. *J Mech Phys Solids.* 2003;51(6):1089–1105.
- [80] Deshpande V, Evans A. Inelastic deformation and energy dissipation in ceramics: a mechanism-based constitutive model. *J Mech Phys Solids.* 2008;56(10):3077–3100.
- [81] Deshpande VS, Gamble EAN, Compton BG, et al. A constitutive description of the inelastic response of ceramics. *J Am Ceram Soc.* 2011;94:s204–s214.
- [82] Paliwal B, Ramesh KT. An interacting micro-crack damage model for failure of brittle materials under compression. *J Mech Phys Solids.* 2008;56(3):896–923.
- [83] Hu G, Liu J, Graham-Brady L, et al. A 3D mechanistic model for brittle materials containing evolving flaw distributions under dynamic multiaxial loading. *J Mech Phys Solids.* 2015;78:269–297.
- [84] Holmquist TJ, Templeton DW, Bishnoi KD. Constitutive modeling of aluminum nitride for large strain, high-strain rate, and high-pressure applications. *Int J Impact Eng.* 2001;25(3):211–231.
- [85] Johnson GR, Holmquist TJ. An improved computational constitutive model for brittle materials. *AIP Conf Proc.* 1994;309:981–984.
- [86] Johnson GR, Holmquist TJ. Response of boron carbide subjected to large strains, high strain rates, and high pressures. *J Appl Phys.* 1999;85(12):8060–8073.
- [87] Shafiq M, Subhash G, Green DJ. An extended Mohr-Coulomb model for fracture strength of intact brittle materials under ultrahigh pressures. *J Am Ceram Soc.* 2016;99(2):627–630.
- [88] Shafiq M, Subhash G. Which One Has More Influence on Fracture Strength of Ceramics: Pressure or Strain Rate? Cham, Switzerland. Conference Proceedings of the Society for Experimental Mechanics Series. 2017.
- [89] Yng Z-Q, Pang B-J, Wang L-W, et al. JH-2 model and its application to numerical simulation on Al₂O₃ ceramic under low-velocity impact. *Explos Shock Waves.* 2010;30(5):463–471.
- [90] Chen WN, Rajendran AM, Song B, et al. Dynamic fracture of ceramics in armor applications. *J Am Ceram Soc.* 2007;90(4):1005–1018.
- [91] Farbaniec L, Hogan JD, Xie KY, et al. Damage evolution of hot-pressed boron carbide under confined dynamic compression. *Int J Impact Eng.* 2017;99:75–84.
- [92] Nittur PG, Maiti S, Geubelle PH. Grain-level analysis of dynamic fragmentation of ceramics under multi-axial compression. *J Mech Phys Solids.* 2008;56(3):993–1017.
- [93] Nie X, Chen WW, Sun X, et al. Dynamic failure of borosilicate glass under compression/shear loading experiments. *J Am Ceram Soc.* 2007;90(8):2556–2562.
- [94] Hu G, Chen CQ, Ramesh KT, et al. Mechanisms of dynamic deformation and dynamic failure in aluminum nitride. *Acta Mater.* 2012;60(8):3480–3490.

- [95] Hu G, Chen CQ, Ramesh KT, et al. Dynamic multi-axial response of a hot-pressed aluminum nitride. *Scr Mater.* 2012;66(8):527–530.
- [96] David NV, Gao XL, Zheng JQ. Ballistic resistant body armor: contemporary and prospective materials and related protection mechanisms. *Appl Mech Rev.* 2009;62(5):050802.
- [97] Compton BG, Gamble EA, Zok FW. Failure initiation during impact of metal spheres onto ceramic targets. *Int J Impact Eng.* 2013;55:11–23.
- [98] Shockey DA, Marchand AH, Skaggs SR, et al. Failure phenomenology of confined ceramic targets and impacting rods. *Int J Impact Eng.* 1990;9(3):263–275.
- [99] Iyer KA. Relationships between multiaxial stress states and internal fracture patterns in sphere-impacted silicon carbide. *Int J Fract.* 2007;146(1–2):1–18.
- [100] Meyer HW. Crack behavior of ballistically impacted ceramic. *AIP Conf Proc.* 2000;505:1109–1112.
- [101] Pickering EG, O'Masta MR, Wadley HNG, et al. Effect of confinement on the static and dynamic indentation response of model ceramic and cermet materials. *Int J Impact Eng.* 2016;110:123–137.
- [102] Han C, Sun CT. A study of pre-stress effect on static and dynamic contact failure of brittle materials. *Int J Impact Eng.* 2000;24(6–7):597–611.
- [103] Sherman D, Brandon DG. The ballistic failure mechanisms and sequence in semi-infinite supported alumina tiles. *J Mater Res.* 1997;12(5):1335–1343.
- [104] Sherman D, Ben-Shushan T. Quasi-static impact damage in confined ceramic tiles. *Int J Impact Eng.* 1998;21(4):245–265.
- [105] Sherman D. Impact failure mechanisms in alumina tiles on finite thickness support and the effect of confinement. *Int J Impact Eng.* 2000;24(3):313–328.
- [106] Anderson CE, RoyalTimmons SA. Ballistic performance of confined 99.5%-Al₂O₃ ceramic tiles. *Int J Impact Eng.* 1997;19(8):703–713.
- [107] Lynch NJ, Bless SJ, Cullis IG, et al. The influence of confinement on the penetration of ceramic targets by KE projectiles at 1.8 and 2.6 km/s. *Int J Impact Eng.* 2006;33(1–12):390–401.
- [108] Savio SG, Ramanjaneyulu K, Madhu V, et al. An experimental study on ballistic performance of boron carbide tiles. *Int J Impact Eng.* 2011;38(7):535–541.
- [109] Rosenberg Z, Dekel E, Hohler V, et al. Penetration of tungsten-alloy rods into composite ceramic targets: experiments and 2-D simulations. *AIP Conf Proc.* 1998;429:917–920.
- [110] Anderson CE, Morris BL. The ballistic performance of confined Al₂O₃ ceramic tiles. *Int J Impact Eng.* 1992;12(2):167–187.
- [111] Liu J, Yuan J. Effects of specimen size and boundary conditions on the penetration depth of metal ceramic structure. *Proc Eng.* 2014;75:71–77.
- [112] Partom Y, Littlefield DL. Validation and calibration of a lateral confinement model for long-rod penetration at ordnance and high velocities. *Int J Impact Eng.* 1995;17(4–6):615–626.
- [113] Chocron IS, Anderson CE, Behner T, et al. Lateral confinement effects in long-rod penetration of ceramics at hypervelocity. *Int J Impact Eng.* 2006;33(1–12):169–179.
- [114] James B. The influence of material properties of alumina on ballistic performance. *Proceedings of the 15th International Symposium on Ballistics, Jerusalem; 1995.* p. 3–10.
- [115] Wei Z, Evans AG, Deshpande VS. The influence of material properties and confinement on the dynamic penetration of alumina by hard Spheres. *J Appl Mech Trans Asme.* 2009;76:5.
- [116] Hauver G, Gooch W, Netherwood P, et al. Variation of target resistance during long-rod penetration into ceramics. Stockholm, Sweden. *Proceedings of International Symposium on Ballistics.* 1992.
- [117] Ning J, Ren H, Guo T, et al. Dynamic response of alumina ceramics impacted by long tungsten projectile. *Int J Impact Eng.* 2013;62:60–74.
- [118] Sarva S, Nemat-Nasser S, McGee J, et al. The effect of thin membrane restraint on the ballistic performance of armor grade ceramic tiles. *Int J Impact Eng.* 2007;34(2):277–302.
- [119] Franzen RR, Orphal DL, Anderson CE. The influence of experimental design on depth-of-penetration (DOP) test results and derived ballistic efficiencies. *Int J Impact Eng.* 1997;19(8):727–737.
- [120] Pan CZ, Zhao ZM, Zhang L, et al. The influence of steel cover thickness on ballistic performance of confined TiC-TiB₂ ceramic tiles against the impact of long-rod tungsten alloy penetrator of 1.4km s⁻¹. *Key Eng Mater.* 2013;544(6):304–309.
- [121] Tabiei A, Nilakantan G. Ballistic impact of dry woven fabric composites: a review. *Appl Mech Rev.* 2008;61(1):010801.
- [122] Rahbek DB, Simons JW, Johnsen BB, et al. Effect of composite covering on ballistic fracture damage development in ceramic plates. *Int J Impact Eng.* 2017;99:58–68.
- [123] Rahbek DB, Johnsen BB. Fragmentation of an armour piercing projectile after impact on composite covered alumina tiles. *Int J Impact Eng.* 2019;133:103332.
- [124] Crouch IG, Appleby-Thomas G, Hazell PJ. A study of the penetration behaviour of mild-steel-cored ammunition against boron carbide ceramic armours. *Int J Impact Eng.* 2015;80:203–211.
- [125] Gassman AH, Paris V, Levin L, et al. Effect of pre-stressing on the ballistic performance of alumina ceramics: experiments and modeling. Daytona Beach, Florida. *International Conference on Advanced Ceramics and Composites.* 2013.
- [126] Serjouei A, Gour G, Zhang X, et al. On improving ballistic limit of bi-layer ceramic-metal armor. *Int J Impact Eng.* 2017;105:54–67.
- [127] Bao YW, Su SB, Yang JJ, et al. Prestressed ceramics and improvement of impact resistance. *Mater Lett.* 2002;57(2):518–524.
- [128] Guiwu L, Changye N, Qiangwei X, et al. Preparation and interface structures of metal-encased SiC composite armors with interpenetrating structure. *Rare Met Mater Eng.* 2011;40(12):2076–2079.
- [129] Holmquist TJ, Johnson GR. Modeling prestressed ceramic and its effect on ballistic performance. *Int J Impact Eng.* 2005;31(2):113–127.
- [130] Zhang R, Han B, Li L, et al. Influence of prestress on ballistic performance of bi-layer ceramic composite armors: experiments and simulations. *Compos Struct.* 2019;227:111258.
- [131] Li JC, Chen XW, Ning F, et al. On the transition from interface defeat to penetration in the impact of long rod onto ceramic targets. *Int J Impact Eng.* 2015;83:37–46.
- [132] Li JC, Chen XW. Theoretical analysis of projectile-target interface defeat and transition to penetration

- by long rods due to oblique impacts of ceramic targets. *Int J Impact Eng.* **2017**;106:53–63.
- [133] Zhang X, Serjouei A, Sridhar I. Criterion for interface defeat to penetration transition of long rod projectile impact on ceramic armor. *Thin Walled Struct.* **2017**;126:266–284.
- [134] Behner T, Heine A, Wickert M. Dwell and penetration of tungsten heavy alloy long-rod penetrators impacting unconfined finite-thickness silicon carbide ceramic targets. *Int J Impact Eng.* **2016**;95:54–60.
- [135] Espinosa HD, Brar NS, Yuan G, et al. Enhanced ballistic performance of confined multi-layered ceramic targets against long rod penetrators through interface defeat. *Int J Solids Struct.* **2000**;37(36):4893–4913.
- [136] Lundberg P, Lundberg B. Transition between interface defeat and penetration for tungsten projectiles and four silicon carbide materials. *Int J Impact Eng.* **2005**;31(7):781–792.
- [137] Westerling L, Lundberg P, Lundberg B. Tungsten long-rod penetration into confined cylinders of boron carbide at and above ordnance velocities. *Int J Impact Eng.* **2001**;25(7):703–714.
- [138] Lundberg P, Renström R, Holmberg L. An experimental investigation of interface defeat at extended interaction time. Interlaken, Switzerland. 19th International Symposium of Ballistics; 2001.
- [139] Lundberg P, Renström R, Andersson O. Influence of length scale on the transition from interface defeat to penetration in unconfined ceramic targets. *J Appl Mech.* **2013**;80(3):031804.
- [140] Andersson O, Lundberg P, Renström R. Influence of confinement on the transition velocity of silicon carbide. Tarragona, Spain. 23rd International Symposium on Ballistics; 2007.
- [141] Lundberg P, Renström R, Andersson O. Influence of confining prestress on the transition from interface defeat to penetration in ceramic targets. *Def Technol.* **2016**;12(3):263–271.
- [142] Holmquist TJ, Anderson CE, Behner T, et al. Mechanics of dwell and post-dwell penetration. *Adv Appl Ceram.* **2013**;109(8):467–479.
- [143] Goh WL, Zheng Y, Yuan J, et al. Effects of hardness of steel on ceramic armour module against long rod impact. *Int J Impact Eng.* **2017**;109:419–426.
- [144] Fabris DCN, Polla MB, Acordi J, et al. Effect of MgO·Al₂O₃·SiO₂ glass-ceramic as sintering aid on properties of alumina armors. *Mater Sci Eng A.* **2020**;781:139237.
- [145] Yin Z, Yuan J, Chen M, et al. Mechanical property and ballistic resistance of graphene platelets/B₄C ceramic armor prepared by spark plasma sintering. *Ceram Int.* **2019**;45(17):23781–23787.
- [146] Meyers MA, Chawla KK. Mechanical behavior of materials. New York: Cambridge University Press; 2009.
- [147] Liu C-Y, Tuan W-H, Chen S-C. Ballistic performance of liquid-phase sintered silicon carbide. *Ceram Int.* **2013**;39(7):8253–8259.
- [148] Shockey DA, Marchand AH, Skaggs SR, et al. Failure phenomenology of confined ceramic targets and impacting rods. *Int J Impact Eng.* **1990**;9(3):263–275.
- [149] Hauver G, Rapacki E, Netherwood P, et al. Interface defeat of long-rod projectiles by ceramic armor, ARL-TR-3950, U.S. Army Research Laboratory. 2005.
- [150] Tan ZH, Han X, Zhang W, et al. An investigation on failure mechanisms of ceramic/metal armour subjected to the impact of tungsten projectile. *Int J Impact Eng.* **2010**;37(12):1162–1169.
- [151] Yuan C, Qin Q, Wang TJ. Simplified analysis of large deflection response of a metal sandwich beam subjected to impulsive loading. *Acta Mech.* **2015**;226(11):3639–3651.
- [152] Chandra N, Nagendra Gopal KV, Raja S. Vibro-acoustic response of sandwich plates with functionally graded core. *Acta Mech.* **2015**;228(8):2775–2789.
- [153] Han B, Zhang Z-J, Zhang Q-C, et al. Recent advances in hybrid lattice-cored sandwiches for enhanced multifunctional performance. *Extreme Mech Lett.* **2017**;10:58–69.
- [154] Yungwirth CJ, Wadley HNG, O'Connor JH, et al. Impact response of sandwich plates with a pyramidal lattice core. *Int J Impact Eng.* **2008**;35(8):920–936.
- [155] Ni CY, Li YC, Xin FX, et al. Ballistic resistance of hybrid-cored sandwich plates: numerical and experimental assessment. *Compos Part A Appl Sci Manuf.* **2013**;46:69–79.
- [156] Ni C, Hou R, Han B, et al. Normal and oblique projectile impact of double-layered pyramidal lattice truss structures filled with ceramic insertions. *J Thermoplast Compos Mater.* **2017**;30(8):1136–1156.
- [157] Zhao ZN, Han B, Li FH, et al. Enhanced bi-layer mosaic armor: experiments and simulation. *Ceram Int.* **2020**;46(15):23854–23866.
- [158] Wadley HNG, Dharmasena KP, O'Masta MR, et al. Impact response of aluminum corrugated core sandwich panels. *Int J Impact Eng.* **2013**;62:114–128.
- [159] Wadley HNG, O'Masta MR, Dharmasena KP, et al. Effect of core topology on projectile penetration in hybrid aluminum/alumina sandwich structures. *Int J Impact Eng.* **2013**;62:99–113.
- [160] Holland CC, Gamble EA, Zok FW, et al. Effect of design on the performance of steel–alumina bilayers and trilayers subject to ballistic impact. *Mech Mater.* **2015**;91:241–251.
- [161] Krell A, Strassburger E. Order of influences on the ballistic resistance of armor ceramics and single crystals. *Mater Sci Eng A.* **2014**;597:422–430.